# *Origin of the Paleoproterozoic basaltic dikes from the central and eastern Dharwar Craton and sills and volcanics from the adjoining Cuddapah Basin, southern India*



**Citation:** Contributions to Mineralogy and Petrology. 2023 Apr 17;178(5):28

**As Published:** https://doi.org/10.1007/s00410-023-02012-0

**Publisher:** Springer Berlin Heidelberg

Contributions to Mineralogy and Petrology (2023) 178:28
https://doi.org/10.1007/s00410-023-02012-0

ORIGINAL PAPER

# Origin of the Paleoproterozoic basaltic dikes from the central and eastern Dharwar Craton and sills and volcanics from the adjoining Cuddapah Basin, southern India

**Nilanjan Chatterjee**[1]

Received: 31 May 2022 / Accepted: 6 April 2023


**Abstract**

Reverse fractionation modeling considering energy-constrained assimilation-fractional crystallization is performed to estimate primary magma compositions, degree of crustal contamination, pressure–temperature of equilibrium with mantle, and potential temperatures for the origin of the Paleoproterozoic (~ 2.37–1.88 Ga) basaltic dikes in central and eastern Dharwar Craton and sills and volcanics in the adjoining Cuddapah Basin, southern India. Mineral thermobarometry indicates that the dikes crystallized at upper crustal conditions (~ 1–6 kbar/ ~ 1120–1210 °C). Hence, the reverse fractionation calculations are performed at low pressures by adding olivine + plagioclase + clinopyroxene, olivine + plagioclase and only olivine in equilibrium with melt, and simultaneously subtracting an upper crustal partial melt in small steps until the melt is multiply saturated with lherzolite at a high pressure. The results indicate that the basalts are 5–30% contaminated, and their enriched light rare earth element (REE) patterns can be attributed to upper crustal assimilation. The upper crust was pre-heated to 665–808 °C during dike emplacement. The primary magmas of all basalts were last equilibrated with spinel lherzolite at 10–16.5 kbar/1291–1366 °C, and they resemble pooled polybaric incremental melts generated along a ~ 1450 °C adiabat. The estimated mantle potential temperatures (1293–1515 °C) are similar to Paleoproterozoic ambient mantle temperatures. All basalts and their primary magmas show lower chondrite-normalized $Dy_N/Yb_N$ ratios than the plume-derived mid-Proterozoic Mackenzie dikes of Canadian Shield, and the primary magmas show flat REE patterns indicating spinel lherzolite melting. The low estimated potential temperatures, low $Dy_N/Yb_N$ ratios, and a spinel-bearing mantle source are at odds with an origin of the basalts from mantle plumes.

**Keywords** Dharwar Craton · Paleoproterozoic dike swarm · Primary magma · Basalt · Lherzolite · Crustal contamination

## Introduction

Flood basalt volcanism is thought to result from high degrees of melting in the upper mantle caused by upwelling of a hot mantle plume from depth (Morgan 1971; Sleep 1990; Davies 1999). The hallmark of a mantle plume is a high potential temperature, $T_P$, defined as the temperature of the mantle if it were to adiabatically decompress and reach the Earth's surface without melting. The excess potential temperature associated with a mantle plume relative to the ambient mantle, $\Delta T_P$, is ~ 100–250 °C (McKenzie and Bickle 1988; Watson and McKenzie 1991; Kinzler and Grove 1992a,b; Presnall et al. 2002; Herzberg et al. 2007; Putirka et al. 2007; Krein et al. 2021). Herzberg et al. (2010) concluded from petrological modeling that the $T_P$ of ambient mantle was ~ 1500–1600 °C at 2.5–3.0 Ga that decreased to the present-day value of ~ 1350 °C in accordance to the Earth's thermal history model of Korenaga (2008). High potential temperatures of ~ 1700 °C estimated for the Archean and Paleoproterozoic komatiites (Herzberg 2022, and references therein) have been used as evidence to support their origin from mantle plumes.

The origin of radiating mafic dike swarms such as the mid-Proterozoic Mackenzie swarm of the Canadian Shield has been linked to mantle plumes (Ernst and Baragar 1992; Baragar et al. 1996). Several researchers contend that the

Communicated by Othmar Müntener.

✉ Nilanjan Chatterjee
nchat@mit.edu

[1] Department of Earth, Atmospheric and Planetary Sciences, Massachusetts Institute of Technology, Cambridge, MA 02139, USA

Published online: 17 April 2023

different Paleoproterozoic (~2.37–1.89 Ga) basaltic dike swarms intruding the central and eastern Dharwar Craton (CDC and EDC, Fig. 1) of the Indian Shield, believed to be remnants of ancient flood basalt provinces, also originated from mantle plumes (Halls et al. 2007; French et al. 2008; Ernst and Srivastava 2008; French and Heaman 2010; Kumar et al. 2012a,b; Belica et al. 2014; Mishra 2015; Stark et al. 2019). Their conclusions are based on

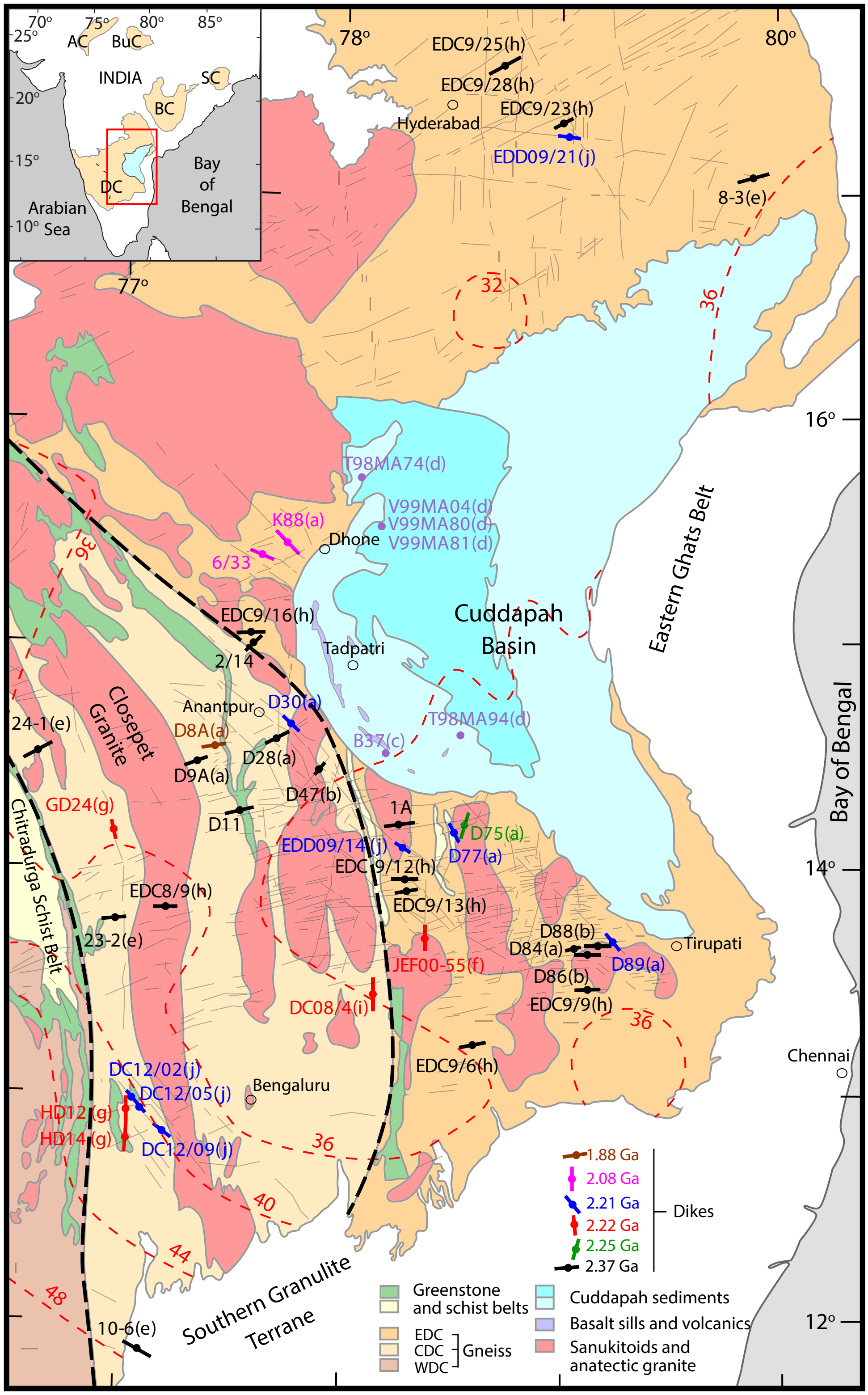


**Fig. 1** Geological map of a part of the Dharwar Craton and Cuddapah Basin (box in inset) after Geological Survey of India (GSI 1998) with boundaries between western (WDC), central (CDC) and eastern (EDC) parts of the craton (thick dashed lines) and for sanukitoids and anatectic granites from Chadwick et al. (2000) and Jayananda et al. (2018), dike swarms (grey lines) from Halls et al. (2007), and Moho depth contours (km, red dashed lines) from Das et al. (2015). Location of the studied samples of dikes, sills and volcanics are shown (letter in parentheses after the sample names refer to sources reporting bulk compositions: **a**—Murty et al. 1987, **b**—Rao et al. 1995, **c**—Chatterjee and Bhattacharji 1998, **d**—Anand et al. 2003, **e**—Halls et al. 2007, **f**—French and Heaman 2010, **g**—Kumar et al. 2012b, **h**, **i** and **j**—Srivastava et al. 2014a,b, 2015). Abbreviations for the cratons are: *AC* Aravalli, *BC* Bastar, *BuC* Bundelkhand, *EDC/CDC/WDC* eastern/central/western Dharwar, and SC—Singhbhum

geometric reconstructions of the piercing points of radial dike swarms across continents using geochronological and paleomagnetic data. However, considering oroclinal bending due to later tectonic deformation, Söderlund et al. (2019) showed that the pre-2.08 Ga swarms were originally linear, and the plume center reconstructions based on the current orientations of the dikes are incorrect. Furthermore, Anand et al. (2003) estimated a $T_P$ of ~ 1500 °C for the ~ 1.89 Ga old sills and volcanics within the adjoining Cuddapah Basin that are genetically related to the ~ 1.89–1.88 Ga old EDC dikes, and explained their result by secular cooling of the Earth without invoking a plume. Sheppard et al. (2017) also presented geological arguments to preclude the involvement of a plume in the origin of the Cuddapah Basin sills and volcanics. In addition, Shellnutt et al. (2018) concluded from isotopic and trace element data that the ~ 1.88 Ga old dikes from the neighboring Bastar Craton, genetically related to the ~ 1.89–1.88 Ga old EDC dikes and Cuddapah Basin sills and volcanics, originated from a subcontinental lithospheric mantle source, not from an asthenospheric source. Srivastava et al. (2015) demonstrated the futility of trace element discrimination diagrams that often indicate incorrect or ambiguous tectonic settings. This study attempts to estimate mantle potential temperatures for the origin of the CDC/EDC dikes and Cuddapah Basin sills and volcanics using their major element compositions. The primary magmas of the basalts and their pressure–temperature (P–T) conditions of equilibrium with mantle are modeled with the reverse fractionation technique that has been previously used for mid-ocean ridge, ocean island, arc, and flood basalts (Till et al. 2012, 2013; Grove et al. 2013; Chatterjee and Sheth 2015; Till 2017; Chatterjee 2021; Krein et al. 2021). There is trace element evidence of upper crustal contamination in the basalts. Hence, the energy-constrained assimilation-fractional crystallization (EC-AFC) formulation of Spera and Bohrson (2001) and Bohrson and Spera (2001) is incorporated in the modeling that provides estimates of the degree of crustal contamination as well as the temperature of the upper crust during magmatism. Abundances of the trace elements including Ni, Rb and the rare earth elements (REE) in the primary magmas are also modeled, providing further insight into the origin the CDC/EDC and Cuddapah Basin basalts.

## Geological setting

The Dharwar Craton (~ 600,000 km$^2$) in southern India is one of the several Archean cratonic blocks that comprise the Indian shield (Naqvi and Rogers 1987) (Fig. 1). It is composed of ~ 3.4–3.0 Ga old tonalite-trondhjemite-granodiorite (TTG) gneisses and Neoarchean greenstone belts with basaltic volcanics that are intruded by late Neoarchean calc-alkaline and potassic granitoids (Friend and Nutman 1991; Chardon et al. 2011; Manikyamba and Kerrick 2012; Jayananda et al. 2013a,b). The oldest rocks representing the cratonic nucleus occur in the western Dharwar Craton (WDC). A steep mylonitic shear zone along the eastern margin of the Chitradurga schist belt has been traditionally considered the eastern boundary of WDC (Swami Nath et al. 1976; Gupta et al. 2003). Based on recent petrologic, geochronologic and isotopic data, the region to the east of the shear zone has been divided into the central and the eastern Dharwar cratonic blocks (CDC and EDC) along the Kolar-Kadiri-Hungund belt (Peucat et al. 2013; Jayananda et al. 2013a). Charnockites near the southern margin of CDC/EDC originated by metamorphism of magmatic protoliths at ~ 2.48 Ga as a result of a collision between the CDC/EDC block and the Southern Granulite Terrane (SGT, Ghosh et al. 2004; Clark et al. 2009).

The EDC is separated from the Eastern Ghats Belt to the east by the crescent-shaped Cuddapah Basin that contains a sequence of gently east-dipping, Proterozoic sedimentary rocks (Nagaraja Rao et al. 1987) (Fig. 1). Near the base of the sequence in the eastern part of the basin, the sediments are intercalated with basaltic pillow lavas in the Vempalle Formation, and basaltic sills and tuffs in the overlying Tadpatri Formation (Sheppard et al. 2017, and references therein). The basaltic exposures are parallel to the arcuate southwestern margin of the basin and coincide with an elliptical region of gravity high (− 55 mGal) surrounded by gravity lows (− 100 mGal) that indicate the presence of a dense (~ 3.0 g cm$^{-3}$) lopolithic intrusion in the upper crust (NGRI 1978; Bhattacharji and Singh 1984; Bhattacharji 1987; Singh et al. 2004). A sill (1899 ± 20 Ma, Anand et al. 2003; 1885.4 ± 3.1 Ma, French et al. 2008) in the lower part and a felsic tuff (1862 ± 9 Ma, Sheppard et al. 2017) in the upper part of the Tadpatri Formation provide evidence for a protracted ~ 30 Myr period of volcanism during sediment deposition. The basin may have started forming before ~ 1.9 Ga by rifting between the EDC and the Napier complex of East Antarctica (Mohanty 2011), and it evolved into a foreland basin after collision with the Eastern Ghats Belt in the late Paleoproterozoic (Collins et al. 2015).

Paleoproterozoic mafic dike swarms of different trends and ages are widespread in the CDC and the EDC (Halls 1982; Murty et al. 1987; Radhakrishna and Joseph 1996; Poornachandra Rao 2005; Halls et al. 2007; French and Heaman 2010; Söderlund et al. 2019; Samal et al. 2021) (Fig. 1). The individual dikes can be traced in length from a few meters to hundreds of kilometers, and their widths vary between 1 m and ~ 400 m. At least nine different dike swarms have been identified (Söderlund et al. 2019; Samal et al. 2021). The dominantly *ENE- to NE-trending (some ESE-trending at the SGT contact) ~ 2.37 Ga old dikes of the Bangalore-Karimnagar swarm* orthogonally cut across the NNW-SSE structural grain of the craton.

These dikes were emplaced within a short interval of < 5 Myr (2369–2365 Ma, Halls et al. 2007; French and Heaman 2010; Kumar et al. 2012a; Liao et al. 2019; Söderlund et al. 2019). The *N- to NNE-trending ~ 2.25 Ga old dikes of the Ippaguda-Dhiburahalli swarm* to the north and south of Cuddapah Basin were also emplaced within a short, ~ 6 Myr time interval (2257–2251 Ma, Nagaraju et al. 2018a; Söderlund et al. 2019). The *N- to NNW-trending ~ 2.22 Ga old dikes of the Kandlamadugu swarm* includes the well-known Kandlamadugu dike to the southwest of Cuddapah Basin and the ~ 400 km long, ~ 2.21–2.22 Ga old, arcuate Nelahalu dike parallel to the western margin of the CDC (French and Heaman 2010; Kumar et al. 2012b; Söderlund et al. 2019). The subparallel *NW- to WNW-trending ~ 2.21 Ga old dikes of the Anantapur-Kunigal swarm* including the Somala dike, and the *NW- to WNW-trending ~ 2.18 Ga old dikes of the Mahabubnagar-Dandeli swarm* including the Dandeli and Bandepalem dikes were emplaced within ~ 30 Myr each other, and the younger dikes probably intruded through some of the older magma pathways (French and Heaman 2010; Nagaraju et al. 2018a,b; Söderlund et al. 2019). Several *NE-, NW- and N-trending ~ 2.08 Ga old dikes of the Devarabanda swarm* around the Cuddapah Basin form a radial swarm with the center inside the basin (Kumar et al. 2015; Söderlund et al. 2019). Two *ENE-trending ~ 1.89–1.88 Ga old dikes of the Hampi swarm* to the west of the basin (Chatterjee and Bhattacharji 2001; Halls et al. 2007) are coeval with the Tadpatri sill within Cuddapah Basin (Anand et al. 2003; French et al. 2008). Some of the ~ 2.08 Ga old dikes and the ~ 1.89–1.88 Ga old dikes are parallel to the older ~ 2.37 Ga and ~ 2.21 Ga old dikes, indicating that the younger dikes were perhaps emplaced by reactivation of older magma pathways and preexisting fractures (cf. Bhattacharji 1987). In addition, several *NW-trending ~ 1.84 Ga old dikes of the Dharmapuri swarm* (Belica et al. 2014) and *NW- to WNW-trending ~ 1.79 Ga old dikes of the Pebbair swarm* (Söderlund et al. 2019) are subparallel to the ~ 2.21 Ga old dikes, and may have also intruded through preexisting magma pathways.

Several researchers have correlated the CDC/EDC dike swarms with swarms on other continents using U–Pb geochronological and paleomagnetic data, and have reconstructed the location of plume centers from which the dike swarms supposedly originated (Halls et al. 2007; French et al. 2008; French and Heaman 2010; Kumar et al. 2012a,b; Stark et al. 2019). These studies suggest that the ~ 2.37 Ga (Bangalore-Karimnagar), ~ 2.21–2.18 Ga (Anantapur-Kunigal and Mahabubnagar-Dandeli) and ~ 1.89 Ga (Hampi) old dike swarms originated from mantle plumes with centers located ~ 300 km west, ~ 1000 km NNW, and ~ 600 km east of the CDC/EDC, respectively. Halls et al. (2007) proposed the location of the ~ 2.37 Ga old plume center to the west of the Dharwar Craton by correlating the Dharwar dikes with the ~ 2.41 Ga old dikes of the Yilgarn Craton. However, Belica et al. (2014) argued against a link between the Yilgarn Craton and the Dharwar Craton at 2.41–2.37 Ga citing age disparity and a ~ 25° latitudinal separation between the two cratons. French and Heaman (2010) also proposed that the Dharwar and Yilgarn dikes are unrelated, and they were emplaced on different continental masses through discrete events. Thus, the locations of the purported plume centers are highly uncertain. Furthermore, Söderlund et al. (2019) argued against the involvement of plumes for the pre-2.08 Ga old CDC/EDC dikes by showing that the swarms were initially linear, and their fan-shaped orientations originated by later tectonic deformation. Hence, the plume center reconstructions are flawed.

## Previous petrological work

The Cuddapah Basin sills and volcanics mostly comprise subalkaline tholeiitic basalts (Chatterjee and Bhattacharji 1998; Anand et al. 2003). A few of the Vempalle samples are alkalic. The major sill complex in the Tadpatri Formation consists of basaltic rocks with mafic xenoliths composed of olivine + orthopyroxene + clinopyroxene + plagioclase (Ol + Opx + Cpx + Pl) near the base, grading into leucocratic gabbro near the top. The minor sills consist of non-cumulate, differentiated basalts. In general, the Cuddapah Basin basalts can be related by fractional crystallization of olivine, clinopyroxene and plagioclase. Thermobarometry shows that the basalts crystallized at a pressure of ~ 5 kbar (~ 18 km depth) and temperatures of 1019–1154 °C (Chatterjee and Bhattacharji 1998). These P–T conditions are consistent with differentiation within a crustal magma chamber under Cuddapah Basin postulated from gravity data (NGRI 1978). The basalts have low loss-on-ignition values indicating minor hydrothermal alteration (Anand et al. 2003). They show negative Nb–Ta anomalies in their incompatible element patterns and high La/Nb (1.3–3.8, cf. primitive mantle: 0.99) and Th/Nb (0.23–1.45, cf. primitive mantle: 0.12) ratios (Anand et al. 2003; McDonough and Sun 1995). Mixing models based on La/Nb and Ce/Y ratios indicate that the non-cumulate basalts comprising most of the Cuddapah Basin lavas and sills are ~ 10–15% contaminated and some minor sills are 20–35% contaminated by the local granitic crust (Anand et al. 2003). The isotopic compositions of the basalts ($\varepsilon$Nd(t) = − 10 to + 1, $^{87}Sr/^{86}Sr_i$ = 0.7056 to 0.7082) are also consistent with upper crustal contamination (Anand et al. 2003). In addition, based on Fe-Nd and REE modeling, Anand et al. (2003) suggested ~ 10–15% partial melting of spinel lherzolite for the generation of the primary magmas of the basalts. They estimated a mantle potential temperature of ~ 1500 °C, and an initially 120 km-thick lithosphere that was thinned to 70 km during magma generation. Moreover, Anand et al. (2003) concluded that the ~ 1500 °C potential temperature can be explained by secular cooling of the Earth without the involvement of a hot mantle plume.

The CDC and EDC dikes are mostly composed of basalts and basaltic andesites. A few have picritic compositions likely due to their cumulate nature. The dikes of all ages show LILE and LREE enrichment and negative Nb–Ta anomalies in normalized incompatible element plots, and high Th/Nb ratios (0.23–0.73) (Kumar et al. 2012a,b; Srivastava et al. 2014a,b, 2015; Liao et al. 2019). In a Th/Yb versus Nb/Yb diagram, the ENE- to NE-trending dikes of the ~2.37 Ga old Bangalore-Karimnagar swarm and the N- to NNW-trending dikes of the ~2.22 Ga old Kandlamadugu swarm plot above the MORB-OIB array and the data trend toward upper continental crust (Kumar et al. 2012a, b). These characteristics have been attributed to AFC-type fractionation of low-Th/Nb parental melts, which are particularly susceptible to Th enrichment and Nb depletion through crustal contamination (Pearce 2008; Kumar et al. 2012a). In addition, the εNd(t) values of the Karimnagar dikes (Bangalore-Karimnagar swarm, −0.7 to +0.6, Liao et al. 2019) and the Nelahalu dike (Kandlamadugu swarm, −2.9 to −1.7, Kumar et al. 2012b) have been attributed to crustal contamination or an isotopically heterogeneous mantle source.

The origin of the ENE- to NE-trending dikes of the ~2.37 Ga old Bangalore-Karimnagar swarm, N- to NNW-trending dikes of the ~2.22 Ga old Kandlamadugu swarm, and NW- to WNW-trending dikes of the ~2.21 Ga old Anantapur-Kunigal swarm were modeled by ~15–25% batch melting of primitive mantle sources (Srivastava et al. 2014a, b, 2015). Furthermore, Srivastava et al. (2015) used chondrite-normalized $Dy_N/Yb_N$ ratios and available petrogenetic models to suggest that the ~2.37 Ga old Bangalore-Karimnagar swarm originated by melting of spinel lherzolite, whereas the ~2.21 Ga old Anantapur-Kunigal, ~2.18 Ga old Mahabubnagar-Dandeli, and ~1.89–1.88 Ga old Hampi swarms originated by melting of transitional spinel-garnet lherzolite.

## Sample locations, age and bulk compositions

Sixteen dike samples were studied in detail for the purpose of mineral thermobarometry. Nine of these samples (D84, D86, D88, 1A, 2/14, D9A, D11, D28, and D47) are from ENE-trending dikes near the western, southwestern and southern margins of Cuddapah Basin (Fig. 1). One of the dikes (D11) has been previously dated at 2369 Ma (dike JEF-99–7, French and Heaman 2010). All of the dikes in this group are inferred to be of the same age and members of the ~2.37 Ga old Bangalore-Karimnagar swarm. Samples D86, D88 and D9A are tholeiitic basalts (Rao et al. 1995), and D88 has a similar bulk composition to several samples (EDC9/6,9,13) analyzed by Srivastava et al. (2014a). D84 is a basaltic andesite, D28 is a picrobasalt, and D47 is a trachyandesite (Murty et al. 1987). In addition, the tholeiitic basalt sample D8A is also from an ENE-trending dike west of the basin (Fig. 1), but it belongs to the younger ~1.89–1.88 Ga old Hampi swarm (1879 Ma, Chatterjee and Bhattacharji 2001). It has a bulk composition (Murty et al. 1987) similar to the Dike-25 sample studied by Halls et al. (2007).

All of the other samples are also tholeiitic basalts. One sample (D75) from an NNE-trending dike near the southwestern margin of Cuddapah Basin (Fig. 1) belongs to the ~2.25 Ga old Ippaguda-Dhiburahalli swarm, though it has a bulk composition (Murty et al. 1987) similar to some ~2.22 Ga old N- to NNW-trending dikes of the Kandlamadugu swarm (Kumar et al. 2012b). Three samples (D89, D77 and D30) are from NW-trending dikes parallel to the southwestern margin of Cuddapah Basin (Fig. 1). These dikes cross-cut the Bangalore-Karimnagar and Ippaguda-Dhiburahalli swarms, and are members of the ~2.21 Ga old Anantapur-Kunigal swarm (French and Heaman 2010). Sample D30 has a variable bulk composition with MgO contents between 8.3 wt% (Murty et al. 1987) and 11.2 wt% (Chatterjee and Bhattacharji 2001). In addition, two samples (6/33 and K88) are also from NW-trending dikes, but they are located near the northwestern margin of Cuddapah Basin (Fig. 1) and they belong to the younger, ~2.08 Ga old Devarabanda radial dike swarm (2083–2080 Ma, Kumar et al. 2015; Söderlund et al. 2019).

## Analytical methods

Textural studies and mineral analyses were performed on a JEOL JXA-733 Superprobe electron probe microanalyzer (EPMA) at Massachusetts Institute of Technology, Cambridge, MA, USA operating with a 15 kV accelerating voltage, a 10 nA beam current, and 1–10 µm beam diameter. Typical counting times were 20–40 s per element that yielded accumulated counts with 1σ standard deviations of 0.3–1.0% for major elements and 1–5% for minor elements from counting statistics. The raw data were corrected for matrix effects with the CITZAF package (Armstrong 1995).

## Petrography and mineral chemistry

The analyzed samples primarily consist of augite and plagioclase with ilmenite and magnetite as common accessory minerals (Fig. 2, Table 1). Minor orthopyroxene and pigeonite are present in some samples. Olivine and Mg-rich amphibole are rare. Most of the samples have equigranular, sub-ophitic and hypidiomorphic textures (Fig. 2a, d).

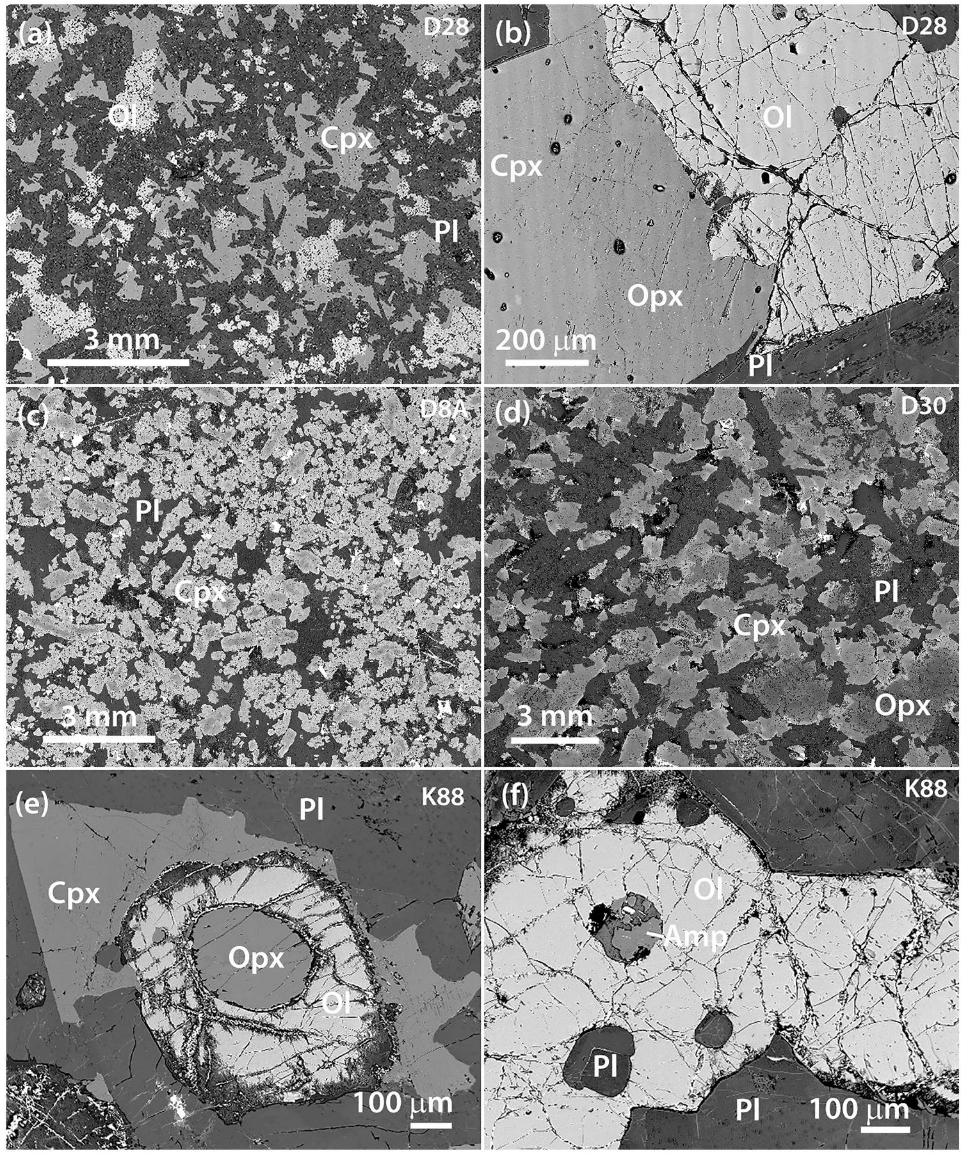


**Fig. 2** Back-scattered electron images of basaltic dike samples (names at upper right corners) from the CDC and EDC showing **a, d** ophitic to sub-ophitic texture dominated by plagioclase laths and clinopyroxene crystals, **b** orthopyroxene between olivine and clinopyroxene, **c** cumulus clinopyroxene with interstitial plagioclase, **e** olivine overgrowth on orthopyroxene, and **f** plagioclase and amphibole inclusions in olivine

## ENE- to NE-trending dikes of the ~ 2.37 Ga old Bangalore-Karimnagar swarm

These dikes are dominantly composed of normally zoned augite and plagioclase with accessory ilmenite, magnetite, titanite, apatite and pyrite. The augite cores in samples D86, D88, 1A, 2/14 and D11 have a restricted composition range ($En_{41-49}Fs_{12-16}Wo_{35-46}$), whereas the augite cores are relatively Fe-rich in D84 ($En_{46}Fs_{21}Wo_{33}$) and Mg-rich in D9A and D28 ($En_{49-50}Fs_{10-14}Wo_{37-41}$) (Fig. 3a, Table S1). Samples D9A and D28 also contain Mg-rich orthopyroxene ($En_{64-71}Fs_{26-31}Wo_{4-5}$) and plagioclase with cores that are more calcic ($An_{79}Ab_{21}$) than in the other samples ($An_{52-68}Ab_{32-49}$) (Fig. 3a, b), and D28 contains olivine with $Fo_{70}$ composition (Fig. 2a, b, Table S1). The high bulk MgO (13.8 wt%) and low $Al_2O_3$ and CaO contents of sample D9A (Murty et al. 1987) are related to excess accumulation of Mg-rich orthopyroxene. Orthopyroxene (Fe-rich) also occurs in D86 ($En_{28}Fs_{67}Wo_4$), and pigeonite (core: $En_{60-64}Fs_{26-39}Wo_{7-10}$) occurs in D84, D86, D88 and D11 (Fig. 3a). The jadeite and aegirine contents of the pyroxenes are < 2.5%. Minor quartz is present in samples D84 and D86. Clinopyroxene is commonly rimmed by actinolite and ferrohornblende. Secondary chlorite, epidote and albite are also present. Clinopyroxene is absent in sample D47 that contains ferroedenite, Fe-rich orthoamphibole and Ca-poor plagioclase ($An_{30}Ab_{70}$).

**Table 1** Mineral assemblages in the CDC and EDC basaltic dikes

| | Latitude/Longitude | Ol | Cpx | Pgt | Opx | Pl | Amp | Mag | Ilm |
|---|---|---|---|---|---|---|---|---|---|
| ENE-trending dikes (~2.37 Ga old Bangalore-Karimnagar swarm) | | | | | | | | | |
| D84 | 13°37′20"N, 78°57′58"E | | X | X | | X | | X | X |
| D86 | 13°35′06"N, 79°01′16"E | | X | X | X | X | | X | X |
| D88 | 13°37′40"N, 79°04′53"E | | X | X | | X | | X | X |
| 1A | 14°09′47"N, 78°12′46"E | | X | | | X | | X | X |
| 2/14 | 13°59′08"N, 77°34′00"E | | X | | | X | | X | X |
| D9A | 14°27′59"N, 77°19′32"E | | X | | X | X | | | X |
| D11 | 14°14′17"N, 77°31′41"E | | X | X | | X | | X | X |
| D28 | 14°33′07"N, 77°39′42"E | X | X | X | X | X | | | X |
| D47 | 14°24′35"N, 77°54′14"E | | | | | X | | | X |
| NNE-trending dike (~2.25 Ga old Ippaguda-Dhiburahalli swarm) | | | | | | | | | |
| D75 | 14°10′33"N, 78°30′00"E | | X | X | | X | | | X |
| NW-trending dikes (~2.21 Ga old Anantapur-Kunigal swarm) | | | | | | | | | |
| D77 | 14°07′51"N, 78°27′02"E | | X | | | X | | | X |
| D89 | 13°39′16"N, 79°07′21"E | | X | | | X | | | X |
| D30 | 14°37′46"N, 77°41′19"E | | X | X | X | X | | X | X |
| NW-trending dikes (~2.08 Ga old Devarabanda swarm) | | | | | | | | | |
| 6/33 | 15°22′46"N, 77°37′18"E | | X | X | | X | | X | X |
| K88 | 15°25′17"N, 77°43′14"E | X | X | | X | X | X | X | X |
| ENE-trending dike (~1.89–1.88 Ga old Hampi swarm) | | | | | | | | | |
| D8A | 14°31′58"N, 77°25′08"E | | X | X | | X | X | X | X |

*Ol* olivine, *Cpx* clinopyroxene, *Pgt* pigeonite, *Opx* orthopyroxene, *Pl* plagioclase, *Amp* amphibole, *Mag* magnetite, *Ilm* ilmenite

### N- to NNE-trending dikes of the ~2.25 Ga old Ippaguda-Dhiburahalli swarm

The NNE-trending dike D75 consists of augite with thick rims of actinolite and ferrohornblende, plagioclase, and accessory epidote, ilmenite and pyrite. The augite and plagioclase cores have compositions of $En_{42}Fs_{23}Wo_{34}$ and $An_{72}Ab_{28}$, respectively (Fig. 3a, b, Table S1). The sample also contains pigeonite ($En_{61}Fs_{28}Wo_{11}$) and minor quartz.

### NW- to WNW-trending dikes of the ~2.21 Ga old Anantapur-Kunigal swarm

Dikes D89 and D77 locally cross-cut the ~2.25 Ga old dike D75. They are mineralogically similar to D75, and are also composed of augite with thick rims of actinolite and ferrohornblende, plagioclase, and accessory epidote, ilmenite and pyrite. However, compared to D75, the augite ($En_{46\text{-}47}Fs_{16}Wo_{37\text{-}38}$) and plagioclase ($An_{60\text{-}64}Ab_{36\text{-}40}$) cores in D89 and D77 are Mg-rich and Ca-poor, respectively (Fig. 3a, b, Table S1). Sample D30 has an equigranular sub-ophitic texture, and it consists of reverse-zoned augite ($En_{52\text{-}55}Fs_{9\text{-}15}Wo_{34\text{-}36}$) and pigeonite ($En_{59\text{-}67}Fs_{22\text{-}31}Wo_{10\text{-}11}$), oscillatory zoned orthopyroxene (core: $En_{73\text{-}80}Fs_{15\text{-}22}Wo_5$, rim: $En_{60}Fs_{36}Wo_4$), and normally zoned plagioclase (core: $An_{68}Ab_{32}$, rim: $An_{25}Ab_{75}$) (Figs. 2d, 3a-d). It also contains secondary orthoamphibole, chlorite and mica, and accessory ilmenite and magnetite.

### Radial dikes of the ~2.08 Ga old Devarabanda swarm

The NW-trending dike K88 is medium-grained and has an ophitic texture. It dominantly consists of augite ($En_{47}Fs_{15}Wo_{39}$) and plagioclase (core: $An_{71}Ab_{29}$) with minor olivine ($Fo_{67}$), orthopyroxene ($En_{68}Fs_{29}Wo_4$) and amphibole (magnesiohastingsite, Mg/(Mg + Fe) = 0.65), and accessory chlorite, ilmenite and magnetite (Fig. 3a, b, Table S1). Orthopyroxene occurs as discrete crystals, exsolution lamellae in augite, and at the rims of olivine and clinopyroxene. Olivine-hosted inclusions of plagioclase, pyroxene and amphibole (Fig. 2e, f) belong to an older generation of basalt, and the olivine overgrowth probably formed through influx of a younger batch of primitive magma. This suggests that dike K88 was probably emplaced by reactivation of an old magma pathway. Another NW-trending dike 6/33 contains augite with lower Mg ($En_{38}Fs_{25}Wo_{38}$) and less calcic plagioclase (core $An_{63}Ab_{37}$) compared to K88 (Fig. 3a, b). It also contains Mg-rich pigeonite ($En_{71}Fs_{19}Wo_{10}$), but it lacks olivine, orthopyroxene and hornblende.

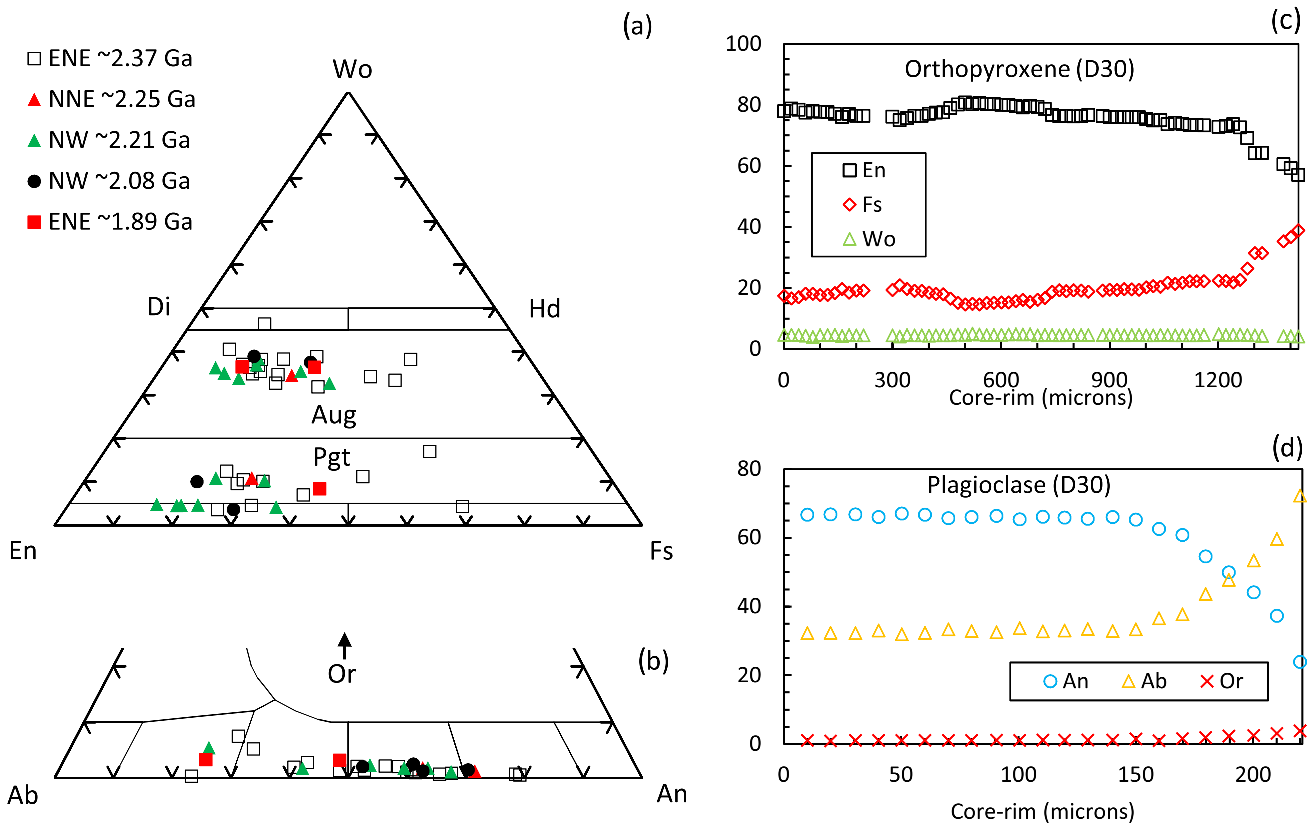


**Fig. 3** Composition of minerals in the CDC and EDC basaltic dikes: **a, c** pyroxenes, and **b, d** plagioclase. **c, d** Compositional variation from core to rim of orthopyroxene and plagioclase in sample D30

### ENE- to NE-trending dikes of the ~ 1.89–1.88 Ga old Hampi swarm

The ENE-trending dike D8A contains abundant cumulus augite (core: $En_{50}Fs_{14}Wo_{36}$) and compositionally zoned plagioclase (core: $An_{49}Ab_{51}$). Augite accounts for > 50% of the rock volume (Fig. 2c). The sample also contains minor pigeonite ($En_{51}Fs_{41}Wo_8$) and hornblende (Mg/(Mg + Fe) = 0.64), secondary albite and mica, and accessory ilmenite and magnetite.

## Thermobarometry

### Methods

The P–T conditions of crystallization were determined with the clinopyroxene-anhydrous liquid thermobarometer of Putirka et al. (1996) using mineral compositions in Table S1 and bulk compositions in Murty et al. (1987) and Rao et al. (1995). The quoted uncertainties in the P–T calculated with this thermobarometer are ± 1.4 kbar and ± 27 °C. Application of this thermobarometer requires that the Cpx is in equilibrium with the bulk (liquid). Equilibrium is assessed from the Cpx-bulk $Fe^{2+}$-Mg distribution coefficient, $K_D(Fe^{2+}\text{-Mg})$, the equilibrium value of which is 0.28 ± 0.08 (Putirka 2008). So, a knowledge of the bulk $Fe^{2+}$ content (or the bulk $Fe^{3+}/Fe$ ratio) is necessary. For samples that contain equilibrium olivine and the equilibrium temperature is independently known, the bulk $Fe^{3+}/Fe$ ratio can be calculated with Eq. 8 of Blundy et al. (2020). Olivine-melt equilibrium is assessed by comparing the observed value of the olivine-bulk Mn-Mg distribution coefficient, $K_D$(Mn-Mg), which is relatively constant over a wide range of P–T–$fO_2$ conditions, with the equilibrium value predicted by the lattice strain model (Blundy et al. 2020). If the observed $K_D$(Mn-Mg) shows disequilibrium, the bulk composition is adjusted by adding or subtracting olivine until olivine is in equilibrium with the bulk (Blundy et al. 2020). This method was attempted on the olivine-bearing samples K88 and D28, the latter with a temperature of 1172 °C determined from Cpx composition only (see below). However, the olivines ($Fo_{67-70}$) in these samples are not in equilibrium with the bulk, as indicated by the higher observed $K_D$(Mn-Mg) values (0.8–1.0) than predicted (0.26–0.27) at 1172 °C, and Eq. 8 of Blundy et al. (2020) yields negative $Fe^{3+}/\sum Fe$ ratios (− 1.35 and − 1.65). Very large corrections (40–45% olivine subtraction) are required to the bulk to bring it in Mn-Mg equilibrium with olivine, and the $Fe^{3+}/\sum Fe$ ratios after correction are unreasonably high (0.36–0.58). So, Blundy et al.'s method was not applied to determine bulk $Fe^{3+}/\sum Fe$ ratios. Instead, the bulk $Fe^{3+}/\sum Fe$ ratios were determined using the spinel-ilmenite equilibrium. First, oxygen fugacity values were calculated from coexisting spinel and ilmenite compositions (program QUILF4, Andersen and Lindsley 1988). Then, Eq. 6b of Putirka (2016a) was used to calculate $\ln(X_{Fe2O3}/X_{FeO})$ of the melt. $Fe^{3+}/Fe^{2+}$ equals $2*X_{Fe2O3}/X_{FeO}$, and $Fe^{3+}/\sum Fe$ is $1/(1+1/(Fe^{3+}/Fe^{2+}))$. For samples in which coexisting spinel and ilmenite are absent, the average bulk $Fe^{3+}/\sum Fe$ ratio of the other samples was used in the calculations.

The P–T were also calculated with the Cpx-composition thermobarometer of Putirka (2008). The T-dependent barometric expression (Eq. 32a) and P-dependent thermometric expression (Eq. 32d) of Putirka (2008) were solved simultaneously to obtain P–T. These equations are based on multiple regression of clinopyroxene compositions obtained from partial melting experiments on basalts in the P–T range of 1 bar-75 kbar/800–2200 °C. The equations use the enstatite-ferrosilite and diopside-hedenbergite components and cation proportions of clinopyroxene calculated on the basis of 6 oxygen atoms. The quoted uncertainties are ± 3.1 kbar and ± 58 °C for clinopyroxene crystallizing from anhydrous melts. In addition, the P–T were also calculated with the random forest machine learning-based algorithms of Higgins et al. (2022) and Jorgenson et al. (2022) that provided independent estimates of the uncertainties. Jorgensen et al. (2022) use the same methodology as Higgins et al. (2022), but they use an expanded dataset that includes Cpx in equilibrium with alkalic liquids. These thermobarometers are also based on clinopyroxene compositions obtained from partial melting experiments on basalts that cover a P–T range of 0.002–30 kbar/750–1250 °C.

The two-pyroxene thermobarometer of Putirka (2008) (uncertainties: ± 3.7 kbar and ± 60 °C) was applied to calculate P–T in sample D30 that contains Cpx and Opx showing equilibrium Fe–Mg distribution ($K_D(Fe^{2+}\text{-}Mg) = 1.09 \pm 0.14$). In addition, samples K88 and D8A contain Mg-rich amphibole, whose compositions were used to calculate temperatures with the thermometer of Putirka (2016b) (uncertainty: ± 30 °C).

## Results

In the ENE-trending ~ 2.37 Ga old Bangalore-Karimnagar dikes, clinopyroxene crystallized at P–T conditions of 0.8–1.5 kbar and 1119–1158 °C, as estimated with the Cpx-anhydrous liquid formulations of Putirka et al. (1996) (Table 2). Using only Cpx compositions, Putirka's (2008) formulations yielded P–T of 1.0–4.9 kbar (± 3.1 kbar) and 1166–1192 °C (± 58 °C) (Table 3). The Higgins et al. (2022) and Jorgenson et al. (2022) methods also yielded low pressures (1 bar-2 kbar), but with lower uncertainties (± 1.1–1.5 kbar, and ± 0.3–2.0 kbar). The temperature estimates are lower with both the methods of Higgins et al. (2022) (1016–1150 °C, ± 20–89 °C) and Jorgenson et al. (2022) (1115–1160 °C, ± 27–88 °C) compared to Putirka (2008), but all three methods have overlapping uncertainties (Table 3). Spinel and ilmenite equilibrated at subsolidus temperatures (457–661 °C) and oxygen fugacity values below the fayalite-magnetite-quartz buffer (ΔFMQ between -0.4 and -3.2), and the calculated range of $Fe^{3+}/\sum Fe$ ratios is 0.06–0.12.

In the NNE-trending dike D75 from the ~ 2.25 Ga old Ippaguda-Dhiburahalli swarm, the estimated P–T of clinopyroxene crystallization are 0.9 kbar and 1119 °C with the Cpx-only formulations of Putirka (2008). The methods of Higgins et al. (2022) (2.0 ± 1.1 kbar, 1032 ± 82 °C) and Jorgenson et al. (2022) (1 bar, 1112 ± 21 °C) yielded similar results.

In the NW-trending ~ 2.21 Ga old Anantapur-Kunigal dikes, clinopyroxene crystallized at P–T conditions of 4.0–5.7 kbar and 1169–1204 °C, as estimated with the Cpx-anhydrous liquid formulations of Putirka et al. (1996) (Table 2). The Cpx-only formulations of Putirka (2008) yielded P–T of 2.6–5.4 kbar (± 3.1 kbar) and 1169–1211 °C (± 58 °C) (Table 3). The Higgins et al. (2022) method yielded similar results (2–7 kbar, ± 0.3–4.0 kbar, 1016–1200 °C, ± 29–76 °C). The Jorgenson et al. (2022) method also yielded similar results (1 bar-2 kbar, ± 0.5–10.0 kbar, 1135–1210 °C, ± 29–79 °C), but very high uncertainties in pressure for sample D30 (Table 3) that may be related to the high $Cr_2O_3$ (> 1 wt%) content of the clinopyroxene (Table S1). In sample D30, the Cpx-Opx thermobarometer of Putirka (2008) yielded P–T of 5.5–5.7 kbar (± 3.7 kbar) and 1150–1178 °C (± 60 °C) (Table 2). Thus, the P–T results for sample D30 with the Cpx-anhydrous liquid, Cpx-only and Cpx-Opx formulations are consistent with each other. Sample D30 also registered a spinel-ilmenite equilibration temperature of 638 °C and ΔFMQ of -1.06 with a corresponding $Fe^{3+}/\sum Fe$ ratio of 0.11.

In the NW-trending dike K88 from the ~ 2.08 Ga old Devarabanda swarm, amphibole crystallized at a temperature of 986 °C, and in dike 6/33 from the same swarm, spinel and ilmenite equilibrated at a temperature of 791 °C and a ΔFMQ value of − 0.49 (Table 2).

In the ENE-trending dike D8A from the ~ 1.89–1.88 Ga old Hampi swarm, clinopyroxene crystallized at P–T conditions of 5.1 kbar and 1202 °C, as estimated with the Cpx-anhydrous liquid formulations of Putirka et al. (1996) (Table 2). With the Cpx-only formulations of Putirka (2008), the P–T are 3.8 kbar (± 3.1 kbar) and 1192 °C (± 58 °C) (Table 3). The Higgins et al. (2022) (5.0 ± 2.4

**Table 2** Mineral-liquid and mineral thermobarometry of the CDC and EDC basalts

| | Compositions used | $K_D(Fe^{2+}$-Mg) | P (kbar) | T (°C)[a] | T (°C)[b] | ΔFMQ[b] | $Fe^{3+}/\sum Fe$[c] |
|---|---|---|---|---|---|---|---|
| ENE-trending dikes (~2.37 Ga old Bangalore-Karimnagar swarm) | | | | | | | |
| D88 | Cpx core, bulk[d] | 0.30 | 1.5 | 1158 | | | |
| | Spl, Ilm | | | | 554 | − 2.32 | 0.06 |
| D86 | Cpx outer core, bulk[d] | 0.31 | 0.8 | 1119 | | | |
| | Spl, Ilm | | | | 661 | − 0.37 | 0.12 |
| D84 | Spl, Ilm | | | | 623 | − 1.97 | 0.06 |
| 1A | Spl, Ilm | | | | 645 | − 2.02 | |
| 2/14 | Spl, Ilm | | | | 642 | − 1.93 | |
| D11 | Spl, Ilm | | | | 457 | − 3.17 | |
| NW-trending dikes (~2.21 Ga old Anantapur-Kunigal swarm) | | | | | | | |
| D77 | Cpx core, bulk[d,e] | 0.37 | 5.0 | 1182 | | | |
| D89 | Cpx core, bulk[d] | 0.34 | 5.7 | 1197 | | | |
| | Cpx core, bulk[e] | 0.31 | 4.0 | 1169 | | | |
| D30 | Cpx outer core, bulk[e] | 0.27 | 4.4 | 1204 | | | |
| | Cpx rim, bulk[e] | 0.36 | 4.1 | 1202 | | | |
| | Spl, Ilm | | | | 638 | − 1.06 | 0.11 |
| | Cpx and Opx outer core | 1.14 | 5.7 | 1178 | | | |
| | Cpx rim, Opx core | 1.16 | 5.6 | 1154 | | | |
| | Cpx rim, Opx outer core | 1.11 | 5.5 | 1150 | | | |
| NW-trending dikes (~2.08 Ga old Devarabanda swarm) | | | | | | | |
| K88 | Amp | | | 986 | | | |
| 6/33 | Spl, Ilm | | | | 791 | -0.49 | |
| ENE-trending dike (~1.89–1.88 Ga old Hampi swarm) | | | | | | | |
| D8A | Cpx core, bulk[d,e] | 0.32 | 5.1 | 1202 | | | |
| | Spl, Ilm | | | | 665 | − 0.54 | 0.16 |
| | Amp | | | 785 | | | |

Formulations: Cpx-bulk (anhydrous liquid): equilb. $K_D(Fe^{2+}$-Mg) = 0.28 ± 0.08, Putirka et al. (1996), Eq. T1 (± 27 °C) and P1 (± 1.4 kbar); Spl-Ilm: Andersen and Lindsley (1988); Cpx-Opx: equilb. $K_D(Fe^{2+}$-Mg) = 1.09 ± 0.14, Putirka (2008), Eq. 37 (± 60 °C) and 38 (± 3.7 kbar); Amp: Putirka (2016b), Eq. 5 (± 30 °C); [a]with Cpx-bulk, Cpx-Opx, or Amp; [b]with Spl-Ilm; [c]with Eq. 6b of Putirka (2016a); bulk compositions from [d]Rao et al. (1995), [e]Murty et al. (1987)

**Table 3** Cpx thermobarometry of the CDC and EDC basalts

| | Composition | P (kbar)[a] | T (°C)[a] | P (kbar)[b] | T (°C)[b] | P (kbar)[c] | T (°C)[c] |
|---|---|---|---|---|---|---|---|
| ENE-trending dikes (~2.37 Ga old Bangalore-Karimnagar swarm) | | | | | | | |
| D88 | Cpx core | 4.9 | 1192 | 2.0 ± 1.4 | 1110 ± 67 | 0.0 ± 0.3 | 1132 ± 30 |
| D86 | Cpx outer core | 4.6 | 1166 | 2.0 ± 1.4 | 1016 ± 89 | 0.0 ± 1.0 | 1115 ± 38 |
| D9A | Cpx core | 1.0 | 1183 | 2.0 ± 1.5 | 1038 ± 47 | 1.0 ± 2.0 | 1160 ± 88 |
| D28 | Cpx core | 2.4 | 1172 | 2.0 ± 1.1 | 1150 ± 20 | 0.7 ± 2.0 | 1148 ± 27 |
| NNE-trending dike (~2.25 Ga old Ippaguda-Dhiburahalli swarm) | | | | | | | |
| D75 | Cpx average | 0.9 | 1119 | 2.0 ± 1.1 | 1032 ± 82 | 0.0 ± 0.0 | 1112 ± 21 |
| NW-trending dikes (~2.21 Ga old Anantapur-Kunigal swarm) | | | | | | | |
| D77 | Cpx core | 3.3 | 1169 | 2.0 ± 0.3 | 1016 ± 70 | 0.0 ± 0.5 | 1135 ± 29 |
| D89 | Cpx core | 5.2 | 1190 | 2.0 ± 1.3 | 1083 ± 76 | 0.0 ± 0.8 | 1142 ± 31 |
| D30 | Cpx core | 2.6 | 1207 | 7.0 ± 4.0 | 1200 ± 29 | 2.0 ± 10.0 | 1210 ± 79 |
| | Cpx outer core | 4.1 | 1211 | 7.0 ± 2.9 | 1193 ± 30 | 0.5 ± 6.3 | 1184 ± 60 |
| | Cpx rim | 5.4 | 1207 | 3.8 ± 2.7 | 1146 ± 40 | 0.0 ± 1.3 | 1140 ± 33 |
| ENE-trending dike (~1.89–1.88 Ga old Hampi swarm) | | | | | | | |
| D8A | Cpx core | 3.8 | 1192 | 5.0 ± 2.4 | 1150 ± 48 | 0.3 ± 2.7 | 1148 ± 37 |

Cpx composition thermobarometers of [a]Putirka (2008), Eq. 32a (± 3.1 kbar) and 32d (± 58 °C); [b]Higgins et al. (2022); [c]Jorgenson et al. (2022)

kbar, 1150 ± 48 °C) and Jorgenson et al. (2022) methods (0.3 ± 2.7 kbar, 1148 ± 37 °C) yielded similar results with lower uncertainties. Amphibole crystallized at a temperature of 785 °C, and spinel-ilmenite equilibrated at a temperature of 665 °C and ΔFMQ of -0.54 with a corresponding $Fe^{3+}/\sum Fe$ ratio of 0.16.

In summary, clinopyroxene crystallized at P–T conditions of 0.8–5.7 kbar and 1119–1211 °C in all samples, estimated using the formulations of Putirka et al. (1996) and Putirka (2008). The machine learning-based algorithms of Higgins et al. (2022) and Jorgenson et al. (2022) yielded similar pressures (1 bar-5 kbar) with lower uncertainties (except for sample D30), but a larger range of temperatures (1016–1210 °C). Spinel and ilmenite equilibrated at subsolidus temperatures (~460–665 °C, excluding 6/33) and ΔFMQ values between -0.5 and -3. The average $Fe^{3+}/\sum Fe$ ratio of the samples is 0.1. These results clearly indicate that the dikes crystallized within the upper crust.

## Primary magma and crustal contamination modeling

### Sample selection

At low pressures such as the ≤ 6 kbar pressures of crystallization calculated above, primitive basalts evolve by crystallizing olivine, followed by Ol + Pl, and then by Ol + Pl + Cpx with decreasing temperature (Kinzler and Grove 1992a). The olivine control line, the Ol-Pl cotectic, and the Ol-Pl-Cpx cotectic together define the fractionation path of the basalt. Any basalt whose composition has been modified by excess crystal accumulation (i.e., a "cumulate" sample) would show displacement from its fractionation path when plotted in the Ol-Pl-Cpx (from Qz) and Ol-Cpx-Qz (from Pl) pseudoternary projections of the basalt tetrahedron according to the methods of Tormey et al. (1987) and Grove (1993). For the purpose of modeling, a total of 88 basalt samples from the literature were considered (Murty et al. 1987; Rao et al. 1995; Chatterjee and Bhattacharji 1998; Anand et al. 2003; Halls et al. 2007; French and Heaman 2010; Kumar et al. 2012a,b; Srivastava et al. 2014a,b, 2015). The bulk composition of each sample and its plagioclase lherzolite multiple saturation point (PL-MSP) at 1 bar-10 kbar pressures predicted by the parameterized expressions of Kinzler and Grove (1992a) were plotted in the pseudoternary projections. The position of the PL-MSP and the constraints of Yang et al. (1996) define the position of the Ol-Pl-Cpx cotectic at different pressures in the projections. Six of the samples plot on their corresponding Ol-Pl-Cpx cotectics, indicating that they represent unmodified basaltic liquids. The other samples are variably displaced from their cotectics. The bulk compositions of these samples were adjusted by subtracting normative olivine so that they plotted on their respective Ol-Pl-Cpx cotectics. Thirty (including the six that plot on their cotectics) of the 88 samples required ≤ 4% normative olivine subtraction, and these were selected for primary magma modeling (Table S2, locations in Fig. 1). The other samples were not selected as their excess crystal contents were deemed too high for meaningful adjustment to the bulk composition.

Six of the selected samples are from inside the Cuddapah Basin: three from the Tadpatri sills (minor sills near Krishnagiri and Yeraguntla-Vempalle, and top part of the major sill near Pulivendla), and three from the Vempalle volcanics near Gattimanikonda (Chatterjee and Bhattacharji 1998; Anand et al. 2003). They plot on their respective Ol-Pl-Cpx cotectics at 1 bar-6.5 kbar pressures (Table 4, S3), consistent with the ~ 5 kbar pressure of crystallization estimated by Chatterjee and Bhattacharji (1998).

From the remainder of the selected samples, 14 are from the ENE- to NE-trending dikes of the ~ 2.37 Ga old Bangalore-Karimnagar swarm (four from CDC, 10 from EDC, Rao et al. 1995; Halls et al. 2007; Srivastava et al. 2014a), five are from the N- to NNW-trending dikes of the ~ 2.22 Ga old Kandlamadugu swarm (three from CDC, two from EDC, French and Heaman 2010; Kumar et al. 2012b; Srivastava et al. 2014b), and five are from the NW- to WNW-trending dikes of the ~ 2.21 Ga old Anantapur-Kunigal swarm (three from CDC, two from EDC, Srivastava et al. 2015). Srivastava et al. (2014a) identified two groups of basalts among the Bangalore-Karimnagar dikes based on chondrite-normalized $La_N/Lu_N$ ratios (~ 2 and > 2). The 14 selected samples of Bangalore-Karimnagar dikes include 11 from the low $La_N/Lu_N$ group and 3 from the high $La_N/Lu_N$ group. The selected dike samples from all swarms plot on their 1 bar-3 kbar Ol-Pl-Cpx cotectics (Table 4, S3), indicating crystallization pressures similar to those obtained from thermobarometry.

The selected samples are all subalkaline tholeiitic basalts (Mg# 37–55) according to the total alkali versus silica classification (Fig. 4a). There is a broad negative correlation between MgO and $FeO^T$ (Fig. 4b). The samples show chemical index of alteration (CIA) values of 37–41, and they are tightly clustered around average unaltered basalt and gabbro in an A-CN-K plot (Nesbitt and Young 1982; Babechuk et al. 2014) (Fig. 4c). Hence, these samples have not been altered by kaolinitization of feldspar, and their bulk K contents have largely remained unchanged since formation. In a Th/Yb versus Nb/Yb diagram (Fig. 4d), the samples plot above the MORB-OIB array and toward upper continental crust, and the trend of the data coincides with a model AFC trend of Pearce (2008). A similar (but less obvious) trend toward upper continental crust is also observed in a Zr/Y versus Nb/Y diagram (Fig. 4e). In a Ce/Y versus La/Nb diagram (Fig. 4f), the data plot along a mixing line between melts of primitive mantle and an average CDC/EDC anatectic granite, as shown previously for the Cuddapah Basin

**Table 4** P–T of crystallization and primary magma equilibration with lherzolite for the CDC, EDC and Cuddapah Basin basalts

| | Crystallization | | | Reverse FC | | | | Reverse EC-AFC | | | | | | | | |
|---|---|---|---|---|---|---|---|---|---|---|---|---|---|---|---|---|
| | | | | | Primary magma[a] | | | | | | | | | Primary magma[a] | | |
| | P | T[b] | Depth | F[c] | P | T | Depth | F[c] | AsmT$_0$[d] | MagT$_1$[e] | M$_a$*/M$_c$[e] | Asm[f] | Crust[g] | P | T | Depth |
| | kbar | °C | km | % | kbar | °C | km | % | °C | °C | | % | | kbar | °C | km |
| ENE- to NE-trending dikes (~2.37 Ga old Bangalore-Karimnagar swarm) | | | | | | | | | | | | | | | | |
| D88 | 3 | 1150 | 11 | 64.1 | 8.5 | 1272 | 31 | 63.3 | 800 | 1179 | 0.391 | 12.2 | a | 11 | 1297 | 38 |
| 8–3 | 0.001 | 1107 | 0.004 | 68.8 | 13 | 1319 | 44 | 67.9 | 665 | 1138 | 0.307 | 17.5 | a | 16 | 1362 | 55 |
| 10–6 | 0.001 | 1102 | 0.004 | 73.0 | 11 | 1302 | 40 | 72.5 | 720 | 1154 | 0.506 | 27.0 | b | 16 | 1363 | 57 |
| 23–2 | 0.5 | 1146 | 2 | 63.3 | 9 | 1280 | 33 | 62.6 | 781 | 1162 | 0.235 | 7.2 | b | 11 | 1305 | 40 |
| 24–1 | 2 | 1151 | 7 | 65.2 | 9.5 | 1286 | 35 | 64.3 | 777 | 1174 | 0.324 | 11.2 | b | 12 | 1311 | 41 |
| EDC9/6 | 0.001 | 1130 | 0.004 | 66.8 | 10 | 1292 | 36 | 65.9 | 750 | 1155 | 0.315 | 12.6 | a | 13 | 1322 | 44 |
| EDC9/12 | 1.5 | 1131 | 5 | 68.5 | 11 | 1303 | 39 | 67.2 | 718 | 1159 | 0.300 | 14.1 | a | 14 | 1340 | 49 |
| EDC9/13 | 2 | 1152 | 7 | 61.0 | 8 | 1268 | 29 | 59.2 | 808 | 1187 | 0.459 | 14.4 | a | 12 | 1311 | 41 |
| EDC9/16 | 2.5 | 1141 | 9 | 67.1 | 9.5 | 1285 | 35 | 65.5 | 755 | 1173 | 0.364 | 15.3 | a | 14 | 1335 | 47 |
| EDC9/25 | 1.5 | 1135 | 5 | 67.4 | 9 | 1279 | 33 | 66.0 | 758 | 1169 | 0.377 | 15.6 | a | 13 | 1328 | 46 |
| EDC9/28 | 1 | 1156 | 4 | 58.0 | 9.5 | 1287 | 35 | 57.7 | 788 | 1169 | 0.219 | 6.3 | a | 11 | 1306 | 39 |
| EDC8/9 | 1 | 1128 | 4 | 67.1 | 13 | 1320 | 44 | 66.5 | 692 | 1151 | 0.233 | 11.8 | b | 15 | 1351 | 52 |
| EDC9/9 | 3 | 1127 | 11 | 65.6 | 8.5 | 1270 | 31 | 62.8 | 780 | 1194 | 0.643 | 29.5 | a | 15 | 1349 | 52 |
| EDC9/23 | 2.5 | 1125 | 9 | 64.8 | 11 | 1299 | 39 | 63.5 | 725 | 1160 | 0.376 | 18.1 | a | 15 | 1348 | 52 |
| N- to NNW-trending dikes (~2.22 Ga old Kandlamadugu swarm) | | | | | | | | | | | | | | | | |
| JEF-00–55 | 2.5 | 1133 | 9 | 65.7 | 9.5 | 1284 | 35 | 64.1 | 760 | 1177 | 0.459 | 20.3 | a | 15 | 1345 | 50 |
| HD12 | 1.5 | 1128 | 5 | 53.7 | 13 | 1314 | 45 | 52.8 | 723 | 1151 | 0.284 | 12.7 | b | 15 | 1338 | 51 |
| HD14 | 0.001 | 1114 | 0.004 | 58.6 | 12 | 1310 | 43 | 57.0 | 710 | 1147 | 0.350 | 17.3 | b | 16 | 1352 | 54 |
| GD24 | 2 | 1137 | 7 | 53.0 | 12 | 1309 | 43 | 50.9 | 735 | 1162 | 0.299 | 12.9 | b | 15 | 1344 | 52 |
| DC08/4 | 1.5 | 1117 | 5 | 72.1 | 10 | 1290 | 36 | 71.4 | 717 | 1155 | 0.383 | 19.2 | a | 14 | 1333 | 47 |
| NW- to WNW-trending dikes (~2.21 Ga old Anantapur-Kunigal swarm) | | | | | | | | | | | | | | | | |
| EDD09/14 | 3 | 1123 | 11 | 74.0 | 12 | 1309 | 41 | 73.6 | 680 | 1153 | 0.296 | 16.2 | a | 15 | 1352 | 52 |
| EDD09/21 | 2.5 | 1130 | 9 | 63.3 | 13 | 1323 | 46 | 61.8 | 716 | 1167 | 0.361 | 18.3 | a | 17 | 1372 | 58 |
| DC12/02 | 2 | 1139 | 7 | 62.3 | 11 | 1303 | 40 | 61.4 | 720 | 1156 | 0.206 | 8.9 | b | 13 | 1327 | 46 |
| DC12/05 | 1 | 1154 | 4 | 54.2 | 11 | 1304 | 40 | 52.3 | 762 | 1165 | 0.169 | 5.6 | b | 13 | 1327 | 46 |
| DC12/09 | 0.001 | 1151 | 0.004 | 49.5 | 11 | 1297 | 38 | 48.1 | 778 | 1162 | 0.162 | 4.8 | b | 12 | 1315 | 43 |
| Vempalle volcanics, Cuddapah Basin (> 1.89 Ga) | | | | | | | | | | | | | | | | |
| V99MA04 | 5 | 1172 | 18 | 56.8 | 8 | 1266 | 29 | 55.7 | 801 | 1185 | 0.225 | 5.9 | a | 10 | 1291 | 36 |
| V99MA80 | 0.001 | 1110 | 0.004 | 64.1 | 9 | 1276 | 33 | 62.3 | 760 | 1159 | 0.519 | 23.4 | a | 14 | 1330 | 47 |
| V99MA81 | 2.5 | 1144 | 9 | 61.5 | 9 | 1277 | 33 | 59.0 | 775 | 1180 | 0.415 | 16.0 | a | 14 | 1332 | 47 |
| Tadpatri sills, Cuddapah Basin (~1.89 Ga) | | | | | | | | | | | | | | | | |
| B37 | 4 | 1152 | 15 | 71.6 | 8.5 | 1274 | 31 | 71.5 | 757 | 1168 | 0.215 | 7.8 | a | 11 | 1304 | 39 |
| T 98MA74 | 5.5 | 1171 | 20 | 63.5 | 8 | 1267 | 29 | 61.9 | 800 | 1206 | 0.418 | 14.0 | a | 12 | 1317 | 43 |
| T98MA94 | 6.5 | 1188 | 24 | 57.7 | 12 | 1315 | 43 | 56.8 | 800 | 1224 | 0.421 | 14.2 | a | 16 | 1359 | 53 |

[a]primary magma (Mg# 73) equilibrated with $Fo_{90}$ olivine; [b]calculated with Eq. 16 of Putirka (2008); [c]degree of fractionation; [d]$T_0$: initial temperature of assimilant (wall rock); [e]$T_1$: magma temperature at which assimilation begins (assimilant reaches solidus assumed at 900 °C), [e]maximum ratio of $M_a$* (mass of partial melt of assimilant mixing with magma) to $M_c$ (mass crystallized from magma); [f]degree of assimilation of crustal melt; [g]average TTG gneiss from EDC (a) and CDC (b)

basalts by Anand et al. (2003). The CDC/EDC samples show similar Th/Nb (0.20–0.60) and La/Nb (1.4–3.7) ratios to the Cuddapah Basin samples (0.23–0.69 and 1.9–2.6) indicating that upper crustal contamination may be similar in the two groups (Fig. 4d, f, Table S2).

In the Th/Yb versus Nb/Yb and Ce/Y versus La/Nb diagrams (Fig. 4d, f), the data plot beyond the range of mixing between primitive melts and lower continental crust, indicating that the lower crust was not the contaminant. A good match with the model AFC trend of Pearce (2008) (Fig. 4d) shows that the primitive melts were probably contaminated

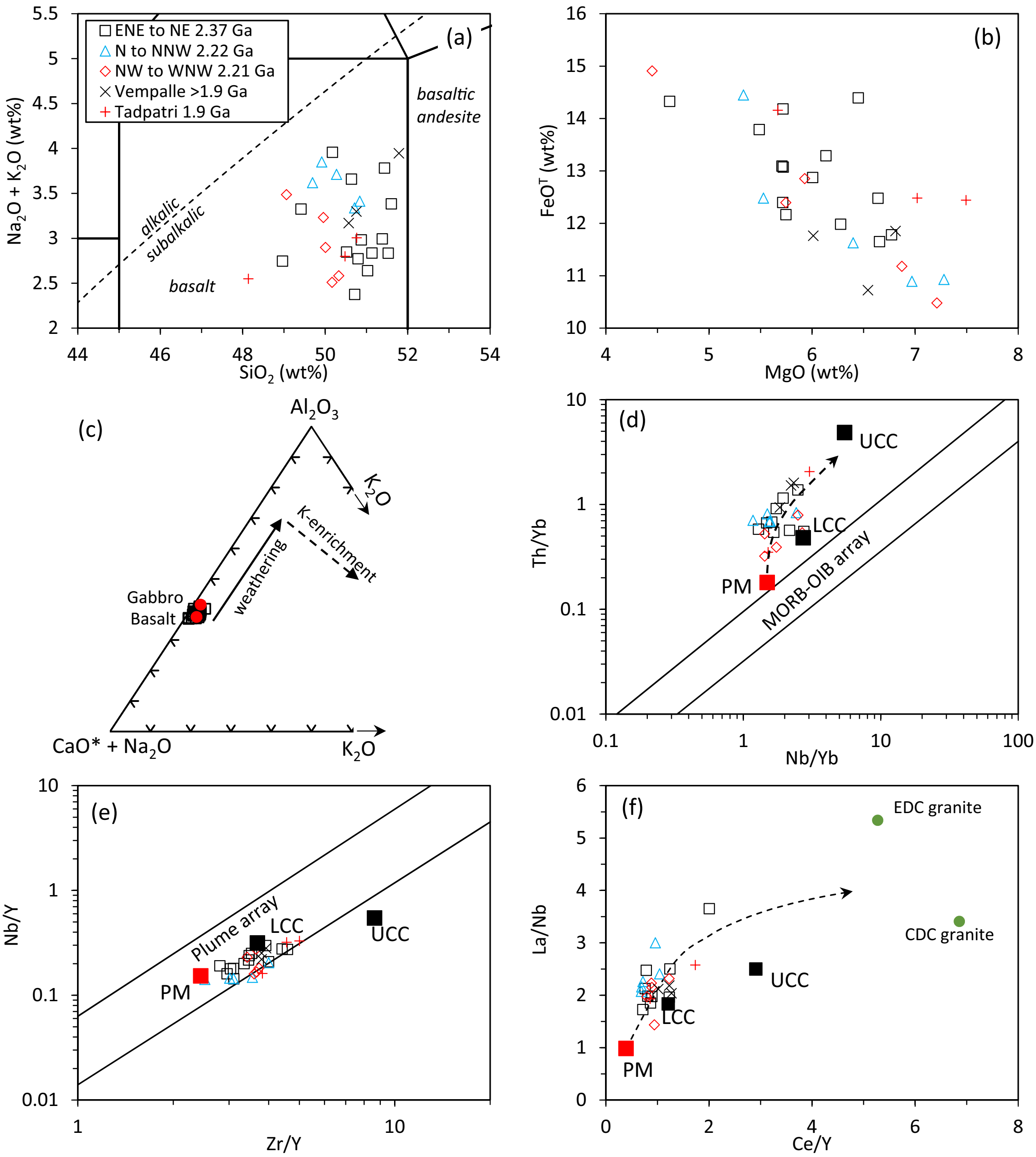


**Fig. 4** Bulk composition of the selected CDC/EDC and Cuddapah Basin basalts (data from Rao et al. 1995, Halls et al. 2007, and Srivastava et al. 2014a for ENE- to NE-trending dikes, French and Heaman 2010, Kumar et al. 2012b, and Srivastava et al. 2014b for N- to NNW-trending dikes, Srivastava et al. 2015 for NW- to WNW-trending dikes, and Chatterjee and Bhattacharji 1998, and Anand et al. 2003 for Vempalle volcanics and Tadpatri sills within Cuddapah Basin), **a** Total alkali versus silica after Le Bas et al. (1986), subalkalic-alkalic boundary from Macdonald and Katsura (1964), **b** MgO versus total FeO, **c** A-CN-K plot, average gabbro and basalt (red dots) from Nesbitt and Young (1982) and Babechuk et al. (2014), **d** MORB-OIB array and dashed line with arrow representing AFC trend from Pearce (2008), **e** Plume array after Condie (2005), **f** Average CDC and EDC anatectic granites (green dots) from Jayananda et al. (2018), dashed line with arrow shows mixing trend of primitive melts with average CDC/EDC granite. **d-f** PM – primitive mantle (McDonough and Sun 1995), and UCC and LCC – upper and lower continental crust (Taylor and McLennan 1995)

with the upper crust through an AFC-type process. However, contamination of the primitive melts during passage through lithosphere containing fusible crustal material acquired by previous subduction cannot be ruled out. In this scenario, the contamination occurred before the primary magma crystallized.

### Calculation method: reverse FC model

Assuming that the CDC/EDC and Cuddapah Basin primary magmas were already contaminated before crystallization during passage through lithosphere, their composition and P–T of equilibration with the metasomatized mantle were determined through simple low-pressure reverse fractional crystallization (Reverse FC) calculations (Till et al. 2012; Chatterjee and Sheth 2015; Till 2017; Krein et al. 2021) (Fig. S1). Starting from the composition of the sample, its low-pressure fractionation path was modeled backward by adding Ol + Pl + Cpx (stage 1), Ol + Pl (stage 2) and Ol-only (stage 3) in small steps (step size < 0.5%) until the melt reached its lherzolite MSP at a high pressure. Equilibrium $Fe^{2+}$-Mg distribution between olivine-liquid ($K_D$($Fe^{2+}$-Mg) = 0.3, Roeder and Emslie 1970) and Cpx-liquid ($K_D$($Fe^{2+}$-Mg) = 0.25), and equilibrium Ca-Na distribution between plagioclase-liquid (Grove et al. 1992) were maintained at each step of the calculation. In stage 1, the melt moved toward the Ol-Cpx sidebar in the Ol-Cpx-Qz projection following the constraints of Yang et al. (1996) that define the intersection of the Ol-Pl-Cpx cotectic with the Ol-Pl cotectic. In stage 2, the melt moved toward the olivine apex in the Ol-Cpx-Qz projection and toward the Ol-Pl sidebar in the Ol-Pl-Cpx projection. In stage 3, the melt moved toward the olivine apex in both projections. The phase proportions and the switching points between stages 1–2 and 2–3 were adjusted so that the melt moved toward its spinel lherzolite MSP (SL-MSP) at high pressures predicted by Till et al.'s (2012) parameterized expressions of experimental data. At the end of the calculation, the melt was in equilibrium with $Fo_{90}$ olivine, and it plotted exactly on its SL-MSP at a specific high pressure. The result was unique, as any deviation from the phase proportions and switching points between stages would result in a melt not on its lherzolite MSP at any pressure, though it may show equilibrium with $Fo_{90}$ olivine (Fig. S1). The trace elements were modeled using the mineral-melt partition coefficients listed in Table S3.

### Calculation method: Reverse EC-AFC model

In AFC, the magma mass changes through mass gained by assimilation of partial melt of wall rock and mass lost by crystallization of the magma. The masses of crystallized and assimilated material depend on the heat budget, which is balanced by heat lost by the magma through cooling and crystallization when the temperature drops below the liquidus, and heat gained by the wall rock through heating and partial melting when the temperature exceeds the solidus. The mass and heat balance constraints are combined together in the AFC formulation (e.g. Thompson et al. 2002). The efficiency of assimilation critically depends on the initial temperature of the crust. Thompson et al. (2002) showed that a picritic magma assimilates tonalitic crust much more efficiently if the crust is initially at 800 °C than at 200 °C. The AFC process is complicated by localized convective heat transfer and dynamic processes including melt segregation by compaction, deformation, and buoyancy instabilities, but these local processes do not have large effects on the overall heat sharing and melting relationships (Annen and Sparks 2002).

Spera and Bohrson (2001) considered energy-constrained AFC (EC-AFC) within an adiabatically sealed system that can be described in terms of a set of coupled ordinary differential equations expressing conservation of energy (enthalpy), total mass, and trace element abundances and isotopic ratios. In this study, the primary magmas were modeled by incorporating the EC-AFC formulation of Spera and Bohrson (2001), and Bohrson and Spera (2001) in the reverse fractionation calculations (Reverse EC-AFC). As in the Reverse FC model, the low-pressure fractionation path was modeled backward by adding Ol + Pl + Cpx (stage 1), Ol + Pl (stage 2) and Ol-only (stage 3) in small steps while maintaining equilibrium $Fe^{2+}$-Mg distribution between olivine-liquid and Cpx-liquid, and equilibrium Ca-Na distribution between plagioclase-liquid. In addition, a partial melt of the upper crustal assimilant was subtracted in each reverse fractionation step as described below.

The EC-AFC calculations were carried out using the updated RK07A_2011_1.xlsm spreadsheet (Spera and Bohrson 2001; Bohrson and Spera 2001). This is a forward modeling approach that requires knowledge of the initial composition and temperature of the magma (i.e., temperature of the primary magma after rising to the upper crust, $T_m^0$), and the initial temperature of the upper crustal assimilant ($T_a^0$). These parameters for each sample were determined through an iterative approach using the K content of the magma. In the first iteration, the input K content of the primary magma was calculated through the Reverse FC method. The bulk compositions of this primary magma and the sample were used to determine $T_m^0$ of the primary magma and $T_m$ of the sample with Eq. 16 of Putirka (2008). The starting value of $T_a^0$ was 300 °C. The $M_a$*/$M_c$ values (ratio of mass of assimilated crustal melt to mass crystallized) as a function of temperature obtained from the EC-AFC forward model were used to subtract the appropriate amounts of partial melt of crustal assimilant in each step of the reverse fractionation. This yielded a tentative estimate of the primary magma considering EC-AFC, whose K content, a recalculated $T_m^0$ (which changed slightly), and an adjusted $T_a^0$ were used as input in the second iteration. The iterations were continued until the K contents of the sample (at $T_m$ of the sample) and the melt in each step of the reverse fractionation matched the K contents predicted by the EC-AFC forward model (Fig. S2). The constraints of the reverse fractionation method ensured that the primary magma plotted on its SL-MSP and the evolving magma remained on its fractionation path. Although the K content was used in the modeling, the Rb contents (where available for the sample) also showed a good match with the Rb contents predicted by the EC-AFC forward model (Fig. S2). The calculations were carried out with an average CDC or EDC TTG gneiss (Jayananda et al. 2018) (Table S2), depending on sample location, as the upper crustal assimilant (Table S2). Partial melts of the assimilant were subtracted in each step using the $M_a$*/$M_c$ value that varies according to energy constraints (in contrast to a constant "r" ratio, DePaolo 1981) during fractionation. In the calculations, the solidus and liquidus temperatures of the upper crustal assimilant were 900 °C and 1000 °C, and the energy parameters were: crystallization enthalpy, $\Delta h_{cry} = 396$ kJ/kg, isobaric specific heat of magma, $C_{p,m} = 1.484$ kJ/kg per K, fusion enthalpy, $\Delta h_{fus} = 270$ kJ/kg, and isobaric specific heat of assimilant, $C_{p,a} = 1.37$ kJ/kg per K (Table 1 of Bohrson and Spera 2001). The equilibration temperature ($T_{eq}$) was assumed as 1000 °C. The gneiss-melt partition coefficients of the trace elements were estimated from their contents in average TTG gneiss and anatectic melt in Jayananda et al. (2018) (Table S2, S3). The basalt-melt elemental partition coefficients were calculated from the estimated proportions of fractionating phases and mineral-melt elemental partition coefficients (Table S2, S3).

### Reverse FC modeling results

The estimated compositions and P–T conditions of equilibrium of the primary magmas with lherzolite for the Reverse FC models are provided in Tables 4 and S2. The primary magmas are high-Mg basalts with MgO contents ranging 10–12 wt%. The fractionation trends for all samples are similar. Stage 1, i.e., the last stage of fractionation, was the longest during which the melts fractionated by an average of 39.9% (from 23.5 to 63.4%, Table S2). Phases were added in average proportions of Ol:Pl:Cpx = 12:49:39 that resulted in an increase in the average Mg# from 44 to 66 (Table S2). During Stage 2 (intermediate stage), the melts fractionated by an average of 21.2% (from 2.3 to 23.5%). Phases were added in average proportions of Ol:Pl = 29:71, resulting in an increase in the average Mg# from 66 to 71. During Stage 3, i.e., the earliest stage of fractionation, the primary magmas fractionated by an average of 2.3%. Only olivine was added, and the average Mg# increased from 70 to 73.

The calculations show that the ~ 1.89 Ga old samples from inside the Cuddapah Basin are 57–72% fractionated, and they were last equilibrated with spinel lherzolite at P–T of 8–12 kbar and 1266–1315 °C (Table 4, S2). The ENE- to NE-trending dike samples from the ~ 2.37 Ga old Bangalore-Karimnagar swarm are 58–73% fractionated, and they were last equilibrated with spinel lherzolite at P–T of 8–12.5 kbar and 1268–1320 °C. The N- to NNW-trending dike samples from the ~ 2.22 Ga old Kandlamadugu swarm are 53–72% fractionated, and they were last equilibrated with spinel lherzolite at P–T of 10–12.5 kbar and 1290–1314 °C. The NW- to WNW-trending dike samples from the ~ 2.21 Ga old Anantapur-Kunigal swarm are 50–74% fractionated, and they were last equilibrated with spinel lherzolite at P–T of 10.5–13 kbar and 1297–1323 °C. All of these results significantly overlap considering their uncertainties (see below), and there are no systematic differences among the different swarms. It is concluded that the samples were last equilibrated with metasomatized spinel lherzolite in the P–T range of 8–13 kbar/1266–1323 °C.

### Reverse EC-AFC modeling results

The estimated compositions and P–T conditions of equilibrium of the primary magmas with lherzolite and the amounts of crustal contamination during fractionation for the Reverse EC-AFC models are provided in Tables 4 and S2, and shown in Figs. 5, 6, and 7. The primary magmas are high-Mg basalts and picrites with MgO contents ranging 10.7–13.2 wt%. The fractionation trends for all samples are similar. The basalts evolved by fractionating and assimilating crustal melt with maximum $M_a$*/$M_c$ ratios between 0.16 and 0.64. Stage 1, i.e., the last stage of fractionation, was the longest during which the melts fractionated by an average of 38.1% (from 24.1 to 62.2%, Table S2). In this stage, phases were added in average proportions of Ol:Pl:Cpx = 13:49:38 that resulted in an increase in the average Mg# from 44 to 65 with concomitant decrease in $SiO_2$ and $Na_2O$, and increase in CaO and $Al_2O_3$ (Fig. 6, Table S2). During Stage 2 (intermediate stage), the melts fractionated by an average of 19.2% (from 4.9% to 24.1%). Phases were added in average proportions of Ol:Pl = 31:69, resulting in an increase in the average Mg# from 65 to 70, decrease in $SiO_2$, CaO and $Na_2O$, and increase in $Al_2O_3$ (Fig. 6). During Stage 3, i.e., the earliest stage of fractionation, the primary magmas fractionated by an average of 4.9%. Only olivine was added, and the average Mg# increased from 70 to 73 as the $SiO_2$, $Al_2O_3$, CaO and $Na_2O$ contents decreased (Fig. 6). The trace element variations of the melts are shown in Fig. 7. The compatible trace element Ni increased with increasing MgO contents (Fig. 7a). The incompatible trace elements Rb and the REE decreased with increasing MgO as also observed for $TiO_2$ and $K_2O$ (Figs. 6b,h, 7b-d).

The calculations show that the ~ 1.89 Ga old samples from inside the Cuddapah Basin were last equilibrated with spinel lherzolite at P–T of 10–15.5 kbar and 1291–1359 °C (Table 4, S2). They are 56–72% fractionated and 6–23% contaminated with crust that was initially at a temperature of 757–801 °C, and assimilation started when the magma was at 1159–1224 °C. The ENE- to NE-trending dike samples from the ~ 2.37 Ga old Bangalore-Karimnagar swarm were last equilibrated with spinel lherzolite at P–T of 10.5–16

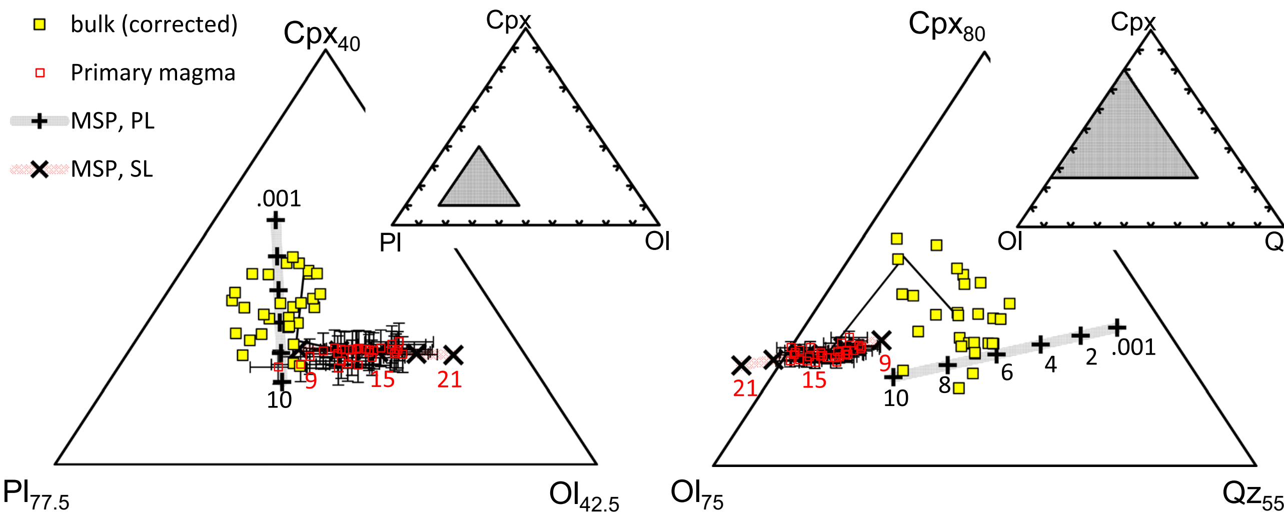


**Fig. 5** Ol-Pl-Cpx and Ol-Cpx-Qz pseudoternary projections from Qz and Pl showing compositions of the selected CDC/EDC and Cuddapah Basin basalts and their primary magmas estimated through Reverse EC-AFC calculations. Also shown are the average fractionation path (black lines, only the average is shown for clarity) and plagioclase lherzolite (PL) MSPs at 1 bar-10 kbar in 2 kbar intervals for the average basalt, and the spinel lherzolite (SL) MSPs at 9–21 kbar in 3 kbar intervals for its primary magma

kbar and 1297–1363 °C. They are 58–73% fractionated and 7–30% contaminated with crust that was initially at a temperature of 665–808 °C, and assimilation started when the magma was at 1138–1194 °C. The N- to NNW-trending dike samples from the ~2.22 Ga old Kandlamadugu swarm were last equilibrated with spinel lherzolite at P–T of 13.5–15.5 kbar and 1333–1352 °C. They are 51–71% fractionated and 13–20% contaminated with crust that was initially at a temperature of 710–760 °C, and assimilation started when the magma was at 1147–1177 °C. The NW- to WNW-trending dike samples from the ~2.21 Ga old Anantapur-Kunigal swarm were last equilibrated with spinel lherzolite at P–T of 12–16.5 kbar and 1315–1366 °C. They are 48–74% fractionated and 5–18% contaminated with crust that was initially at a temperature of 680–778 °C, and assimilation started when the magma was at 1153–1165 °C.

All of these results significantly overlap considering their uncertainties (see below), and there are no systematic differences among the different swarms. Considering all samples, the P–T range for last equilibration with spinel lherzolite was 10–16.5 kbar/1291–1366 °C. These P–T conditions are higher than the P–T estimated through the Reverse FC models. The samples are mostly ≤ 20% contaminated except for three samples, one from the Vempalle volcanics of Cuddapah Basin and two from the ENE- to NE-trending ~2.37 Ga old Bangalore-Karimnagar dikes, that are 23–30% contaminated. The upper crust was already at high temperatures (665–808 °C) at the time the dikes, sills and volcanics were emplaced.

## Uncertainties

The uncertainties in the estimated compositions and P–T of primary magmas arise from the uncertainties in the equilibrium mineral-melt $K_D(Fe^{2+}\text{-}Mg)$ coefficients, and the mantle olivine composition that may vary between $Fo_{88}$ and $Fo_{92}$. If the primary magma is allowed to equilibrate with olivine compositions between $Fo_{88}$ and $Fo_{92}$ using fixed $K_D(Fe^{2+}\text{-}Mg)$ values, the uncertainty in the Mg# of the primary magma is ± 6% (Mg# range: 68.5–77.5), and the uncertainties in the MgO and FeO contents of the primary magma are ± 12% and ± 10% (represented by error bars in Figs. 5–7). These uncertainties are larger than the uncertainties calculated by changing the $K_D(Fe^{2+}\text{-}Mg)$ values. For example, a ± 10% change in the Ol-melt and Cpx-melt $K_D(Fe^{2+}\text{-}Mg)$ values results in a ± 3% change in MgO and ± 6% change in FeO of the primary magma for the most fractionated (73%) sample EDD09/14. For less fractionated samples such as GD24 (51% fractionated), a ± 10% change in the Ol-melt and Cpx-melt $K_D(Fe^{2+}\text{-}Mg)$ values results in a ± 2% change in MgO and ± 3% change in FeO of the primary magma. Using higher values of $K_D(Fe^{2+}\text{-}Mg)$ results in an increase in FeO and decrease in MgO, and the primary magma (Mg# 71.2–71.9) equilibrates with $Fo_{88.2\text{–}88.6}$ olivine. Using lower values of $K_D(Fe^{2+}\text{-}Mg)$ results in a decrease in FeO and increase in MgO, and the primary magma (Mg# 74.7–74.0) equilibrates with $Fo_{91.6\text{–}91.3}$ olivine.

Multiple regression of lherzolite saturated melt compositions in experiments indicate that the P–T values at SL-MSP are accurate within ± 1.5 kbar and ± 11 °C (Till et al. 2012; Krein et al. 2021). However, the uncertainties in the P–T

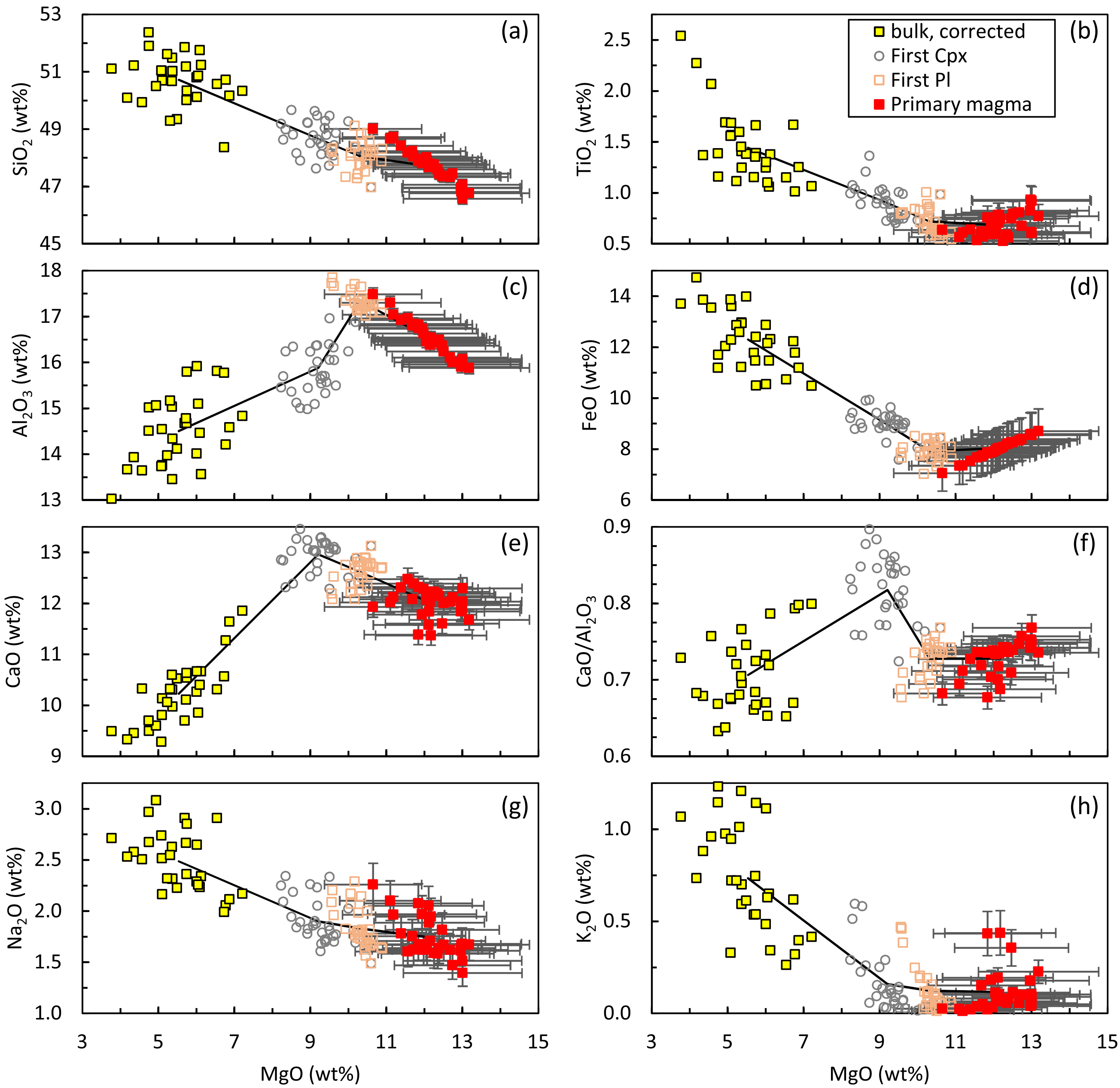


**Fig. 6** Bivariate plots showing the variation of major oxides and $CaO/Al_2O_3$ with MgO for the selected CDC/EDC and Cuddapah Basin basalts and their parental and primary magmas estimated through Reverse EC-AFC calculations. The fractionation path of each basalt is distinct but similar. For clarity, only an average fractionation path (black lines) is shown. Melts labeled “First Pl” and “First Cpx” correspond to initiation of plagioclase and Cpx crystallization

of multiple saturation are larger if the primary magma is allowed to equilibrate with olivine compositions between $Fo_{88}$ and $Fo_{92}$. In this case, the average uncertainties in pressure and temperature are ± 15% and ± 3%, respectively (e.g., 15 ± 2.3 kbar, 1350 ± 40 °C), and the average uncertainty in the estimated crustal assimilation is ± 20% (e.g., 10 ± 2%).

## Discussion

### Crustal contamination

Application of EC-AFC in the reverse fractionation modeling shows that the amount of upper crustal contamination in the Cuddapah Basin basalts is 6–23% (Table 4). This is in good agreement with the model mixing of 10–35% granitic crust with the Cuddapah Basin primary melts based on

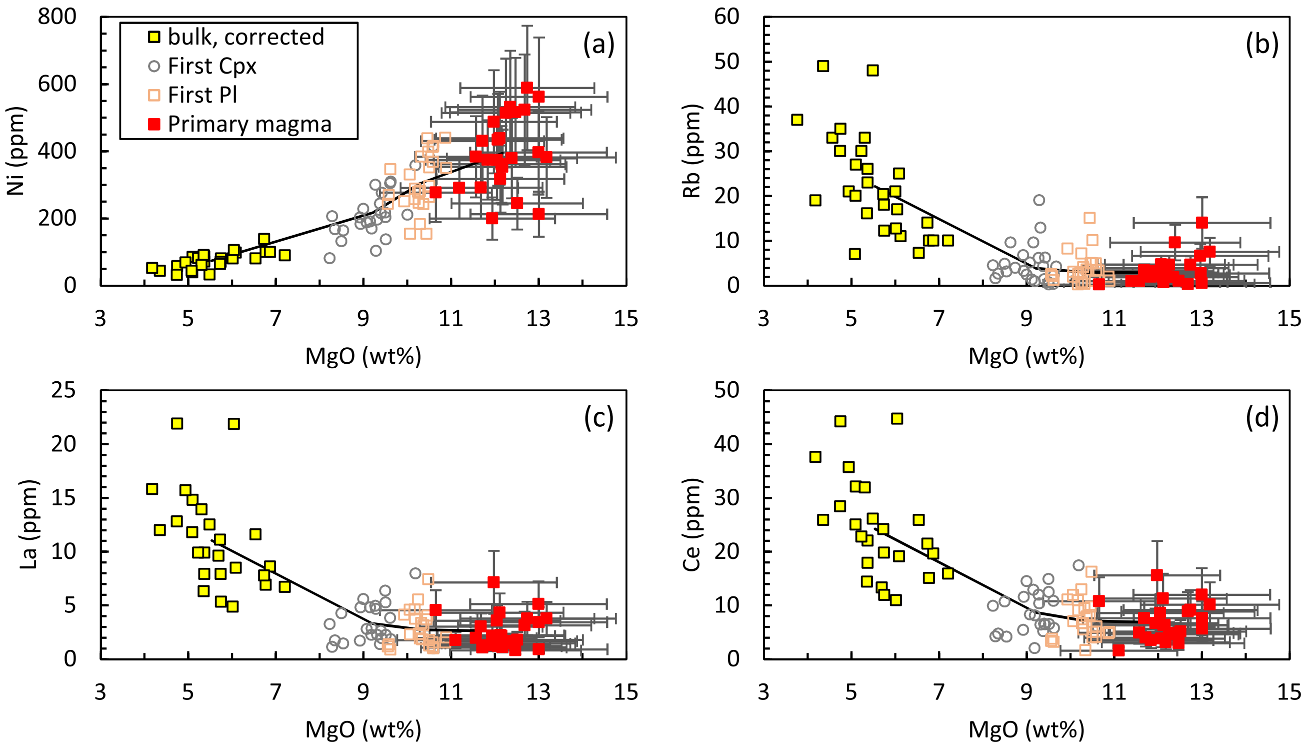


**Fig. 7** Bivariate plots showing the variation of trace elements with MgO for the selected CDC/EDC and Cuddapah Basin basalts and their parental and primary magmas estimated through Reverse EC-AFC calculations. The fractionation path of each basalt is distinct but similar. For clarity, only an average fractionation path (black lines) is shown. Melts labeled "First Pl" and "First Cpx" correspond to initiation of plagioclase and Cpx crystallization

La/Nb and Ce/Y ratios by Anand et al. (2003). The CDC/EDC dikes also show 5–30% upper crustal contamination. An important result of the Reverse EC-AFC modeling is that the upper crust was already heated to high temperatures (665–808 °C) during emplacement of the various dike swarms. Such thermal priming of the crust has been attributed to persistent magmatism for the Steens basalts in the Columbia River flood basalt province (Moore et al. 2018, 2020). According to field observations, the ~ 2.37 Ga old Bangalore-Karimnagar dikes cross-cut an older set of mafic dikes (Padmakumari and Dayal 1987; Kumar and Bhalla 1983). The CDC crust was probably pre-heated to high temperatures by the intrusion of the older dikes. Furthermore, there is evidence of a major thermal pulse at ~ 2.5 Ga followed by slow cooling to ~ 2.4 Ga in the CDC/EDC (Jayananda et al. 2011, 2013b; Peucat et al. 2013). For example, in the southern part of CDC, garnet dated at 2439 ± 36 Ma and 2435 ± 56 Ma in metapelite and calc-silicate gneiss grew under granulite facies conditions (Jayananda et al. 2013b). Thus, the crust was at high temperatures ~ 65 Myr (at least ~ 10 Myr considering uncertainties) before the emplacement of the ~ 2.37 Ga old dikes. The CDC/EDC crust was also thermally primed by the intrusion of the Ippaguda-Dhiburahalli swarm (~ 2.25 Ga) ~ 5 Myr before the emplacement of the Kandlamadugu swarm (~ 2.22 Ga), and the Anantpur-Kunigal swarm (~ 2.21 Ga) was emplaced another ~ 10 Myr later. The prevailing high temperatures of the crust is evident from the presence of anatectic granites such as the 2221 ± 99 Ma old Yelagatti granitoid in northern EDC (Rogers et al. 2007). The EDC crust was also probably thermally primed by the intrusion of the Devarabanda swarm at ~ 2.08 Ga before the eruption of the Vempalle volcanics (> 1.89 Ga) and intrusion of the Tadpatri sills (~ 1.89 Ga) within Cuddapah Basin.

## Potential temperatures

The apparent potential temperatures ($T_P$*, Krein et al. 2021) for the origin of the CDC/EDC and Cuddapah Basin primary magmas, estimated from the P–T of multiple saturation with spinel lherzolite with the Reverse EC-AFC models (10–16.5 ± 2.3 kbar, 1291–1366 ± 40 °C) and an adiabatic slope (dT/dP) of 1.5 °C/kbar, are 1233–1385 °C. The Reverse FC models indicate lower P–T of multiple saturation with spinel lherzolite, reflecting equilibrium with a metasomatized mantle. The Reverse FC results were not used to estimate potential temperatures. The true potential temperature ($T_P$) depends on the style and degree of melting (Krein et al. 2021). To assess the approximate degree of melting, the compositions of the calculated CDC/EDC and Cuddapah Basin primary magmas based on the Reverse EC-AFC models are compared with model melts of spinel lherzolite (Behn and Grove 2015) (Fig. 8). The N- to NNW-trending dike samples from the ~ 2.22 Ga old Kandlamadugu swarm show a restricted range of FeO and $SiO_2$, indicating ~ 10–20% melting at 15–20 kbar pressure according to the isobaric batch melting models. The NW- to WNW-trending dike samples from the ~ 2.21 Ga old Anantapur-Kunigal swarm show a restricted range of $Na_2O$ and $CaO/Al_2O_3$, indicating 15–20% batch melting at pressures between ~ 15 kbar and > 20 kbar. Most of the ENE- to NE-trending dike samples from the ~ 2.37 Ga old Bangalore-Karimnagar swarm are similar to the NW- to WNW-trending Anantapur-Kunigal dike samples. Hence, their pressure and degree of batch melting are probably similar. The Cuddapah Basin samples show a negative correlation between FeO and $Na_2O$, and positive correlations between $SiO_2$ and $Na_2O$, and between FeO and $CaO/Al_2O_3$. These trends also suggest 10% to > 20% batch melting at pressures between ~ 12 kbar and > 20 kbar. However, all CDC/EDC and Cuddapah Basin primary magmas estimated above probably represent pooled melts as their average compositions are similar to a pooled melt generated by polybaric incremental melting at pressures between 26 and 9 kbar along a 1450 °C adiabat (Behn and Grove 2015). Assuming ~ 10–20% melting, $T_P$ may be ~ 60–130 °C higher than the estimated $T_P$* for narrow to fully pooled melts (Table S2 of Krein et al. 2021). Thus, the range of $T_P$ may be 1293–1515 °C.

The estimated $T_P$ values of all samples are similar to predicted ambient mantle temperatures in the Paleoproterozoic according to various thermal history models of the Earth (see Fig. 10 of Herzberg 2022). Even the highest estimated $T_P$ (1515 °C) is not higher than the Paleoproterozoic ambient mantle temperature predicted by the model of Korenaga

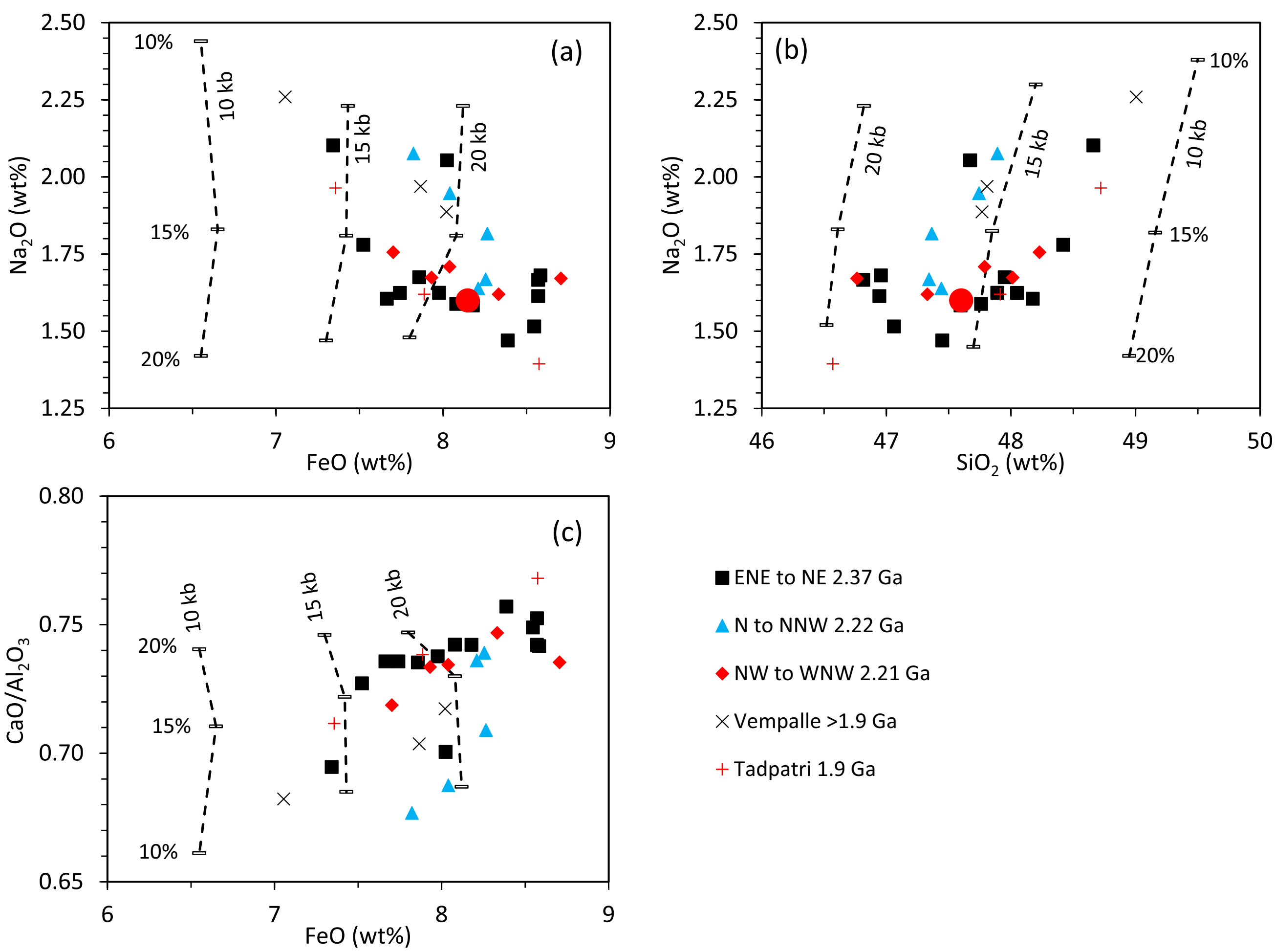


**Fig. 8** Compositions of the CDC/EDC and Cuddapah Basin primary magmas compared with model melts of spinel lherzolite (Behn and Grove 2015). Dashed lines: isobaric batch melts at 10, 15 and 20 kbar; red dot in **a** and **b**: pooled polybaric incremental melt generated along a 1450 °C adiabat

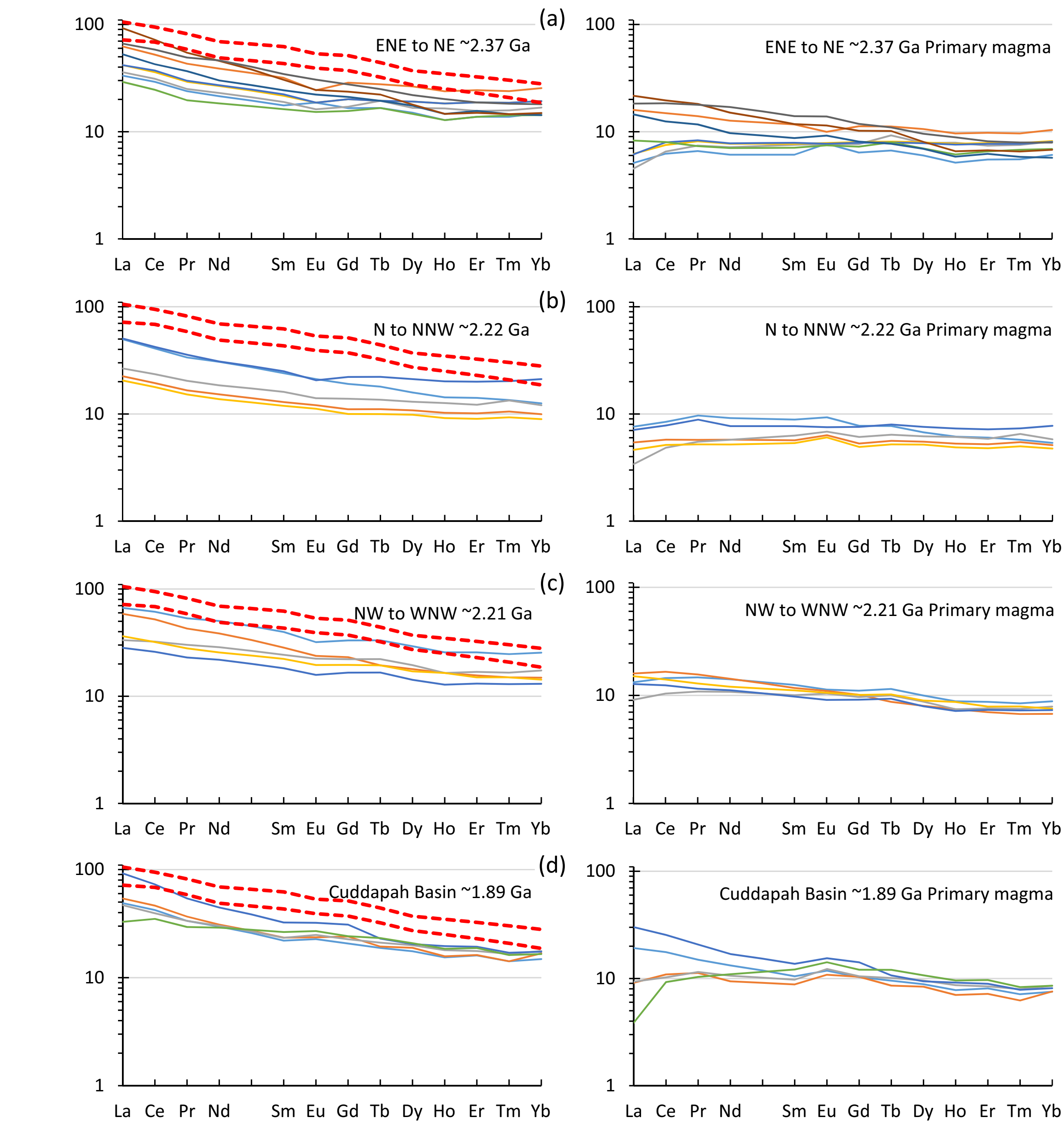


**Fig. 9** Chondrite-normalized (McDonough and Sun 1995) REE patterns of basalts and their primary magmas (Reverse EC-AFC models) from **a** ENE- to E-trending, **b** N- to NNW-trending, and **c** NW- to WNW-trending dikes of the CDC/EDC, and **d** sills and flows within the Cuddapah Basin. The range for the Mackenzie dikes (Baragar et al. 1996) is shown by two dashed lines

(2008). Thus, there is no indication of a mantle plume based on the above estimates of $T_P$. However, magma may lose heat during its passage through the lithosphere, especially in dike swarms where lateral flow may be important (Ernst and Baragar 1992; Ernst et al. 2019). In this case, the above $T_P$ estimates may be lower than the actual $T_P$. To further assess the origin of the CDC/EDC and Cuddapah Basin basalts, their REE patterns are compared in the following section with the Mackenzie dikes of Canadian Shield that are evidently derived from a mid-Proterozoic mantle plume (Ernst and Baragar 1992; Baragar et al. 1996).

## Plume origin?

The Mackenzie dikes are composed of subalkaline tholeiitic basalts with Mg# ranging 41–50 (averages in Table 6 of Baragar et al. 1996), similar to the CDC/EDC and Cuddapah Basin basalts considered above (Mg# 37–55). They also consist of plagioclase, pyroxene, and Fe-Ti oxides with rare olivine, and their estimated P–T of emplacement are ≤ 5 kbar/ ~ 1025–1225 °C (Baragar et al. 1996). Thus, the major element compositions and emplacement conditions of the Mackenzie dikes are similar to the CDC/EDC dikes and Cuddapah Basin sills.

The incompatible trace element patterns of the Mackenzie basalts show LILE enrichment relative to HFSE, LREE enrichment relative to HREE, enriched Nb-Ce plateaus, and negative anomalies for Sr, Ti and K (Baragar et al. 1996). Their εNd(t) values are mostly between 0 and + 2, indicating little contamination with the continental crust. By comparison, all CDC/EDC and Cuddapah Basin basalts show prominent negative anomalies for Nb, but not for K (Srivastava et al. 2015), and they show evidence of upper crustal contamination in incompatible trace element ratio diagrams (Fig. 4d, e, f). Their εNd(t) values (–10 to + 1) also suggest variable degrees of contamination (Anand et al 2003; Kumar et al. 2012b; Liao et al. 2019). Compared to the Mackenzie basalts, the REE abundances of the CDC/EDC and Cuddapah Basin basalts are lower, but they also show LREE enrichment relative to HREE (Figs. 9, S3). When the basalts are corrected only for fractionation (primary magmas with Reverse FC, Table S2), their chondrite-normalized $La_N/Sm_N$ and $Dy_N/Yb_N$ ratios remain largely unchanged (Fig. S3). But when they are corrected for fractionation and upper crustal assimilation (primary magmas with Reverse EC-AFC, Table S2), their $La_N/Sm_N$ ratios decrease while their $Dy_N/Yb_N$ ratios remain similar (Figs. 9, 10, S3). High $La_N/Sm_N$ ratios of basalts may result from upper crustal contamination or through clinopyroxene-dominated fractional crystallization occurring at high pressures. Since the thermobarometric calculations do not show evidence of high-pressure crystallization, the elevated $La_N/Sm_N$ ratios of the CDC/EDC and Cuddapah Basin basalts are probably due to upper crustal contamination.

Compared to the CDC/EDC and Cuddapah Basin basalts, the $Dy_N/Yb_N$ ratios of the Mackenzie basalts are distinctly higher (Fig. 10), indicating a deeper origin from a garnet-bearing source (Baragar et al. 1996). By contrast, the lower $Dy_N/Yb_N$ ratios of all CDC/EDC and Cuddapah Basin basalts and their primary magmas, and the flat REE patterns of most of the primary magmas (Reverse EC-AFC models) (Figs. 9, S3) indicate melting of a primitive spinel lherzolite source (see modeling by Shellnutt et al. 2018). Some of the primary magmas even show $La_N/Sm_N < 1$ (Fig. 10), indicating the possibility of a depleted source. This does not preclude origin from a plume because plumes are chemically heterogeneous, often containing both enriched and depleted components (White 2010). However, neither the CDC/EDC and Cuddapah Basin basalts nor their primary magmas exhibit a deep melting signature such as the high $Dy_N/Yb_N$ ratios observed in the plume-derived Mackenzie

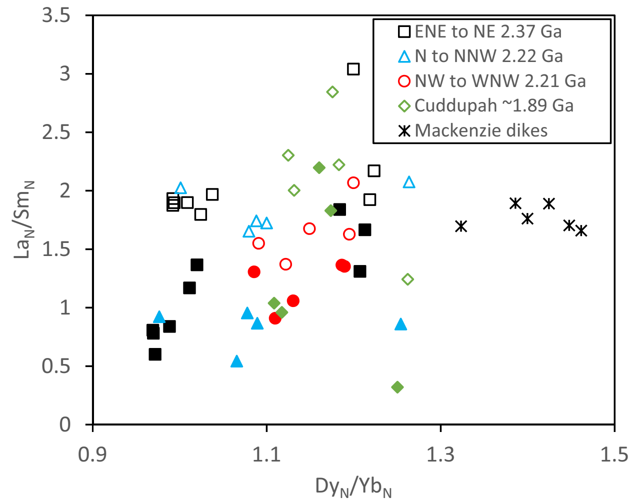


**Fig. 10** Bivariate plot of chondrite-normalized (McDonough and Sun 1995) REE ratios for the CDC/EDC dikes, Cuddapah Basin sills and flows, and Mackenzie dikes (Baragar et al. 1996). The filled symbols represent primary magmas (Reverse EC-AFC models)

basalts (Fig. 10). Thus, there is no indication from the REE data of a plume-related origin for any of the CDC/EDC and Cuddapah Basin basalts.

The non-plume origin for all CDC/EDC dikes and Cuddapah Basin sills and volcanics agrees with the studies of Anand et al. (2003), Sheppard et al. (2017), Shellnutt et al. (2018), and Söderlund et al. (2019), whose conclusions are based on petrological modeling, and geological, isotopic, trace element, and field structural data. The ~ 1300–1500 °C potential temperatures estimated in this study (Reverse EC-AFC models) and Anand et al. (2003) are lower than the estimated temperatures (> 1575 °C) for the late Archean komatiitic amphibolites from Kolar schist belt (CDC-EDC boundary, Rajamani et al. 1985) that may have originated from a mantle plume. Herzberg (2022) also concluded that Archean and Paleoproterozoic komatiites with temperatures of ~ 1700 °C may have originated from mantle plumes, but the ~ 1550 °C temperatures estimated for the ~ 1.88 Ga tholeiitic intrusives of the Circum-Superior LIP indicate that a plume was not involved in their origin. Dike emplacement is controlled by factors such as crustal stress, crustal heterogeneity, magma viscosity and intrusion rates (Rivalta et al. 2015; Kjøll et al. 2019). A discussion of these mechanisms is beyond the scope this paper.

## Conclusions

Mineral thermobarometry indicates that the CDC/EDC dikes around Cuddapah Basin crystallized at upper crustal P–T conditions of ~ 1–6 kbar and ~ 1120–1210 °C. Spinel and ilmenite equilibrated at subsolidus temperatures

(~460–660 °C) and oxygen fugacity values below the fayalite-magnetite-quartz buffer (ΔFMQ values of -0.5 to -3) that correspond to bulk $Fe^{3+}/\sum Fe$ ratios of 0.06–0.16. Thirty selected CDC/EDC and Cuddapah Basin basalts of different ages from the literature (with minor correction in bulk composition for crystal accumulation) plot on their Ol-Pl-Cpx cotectic boundaries at 1 bar-6.5 kbar pressures, consistent with the pressure estimates from mineral thermobarometry. Primary magmas modeled through reverse fractionation calculations incorporating crustal assimilation (Reverse EC-AFC) show that they were last equilibrated with spinel lherzolite at P–T conditions of 10–16.5 kbar (±2.3 kbar) and 1291–1366 °C (±40 °C). Considering EC-AFC, the models show that the basalts are mostly ≤20% contaminated with the upper crust except for three samples that are 23–30% contaminated. The upper crust was thermally primed to high temperatures (665–808 °C) at the time of emplacement of the different dike swarms. A comparison with model melts of spinel lherzolite (Behn and Grove 2015) shows that basalts can be generated by ~10% to >20% batch melting at ~12–25 kbar pressures. The estimated primary magmas all basalts probably represent polybaric incremental pooled melts generated along a ~1450 °C adiabat. The estimated range of mantle potential temperatures is 1293–1515 °C. These potential temperatures are not higher than ambient mantle temperatures in the Paleoproterozoic according to different thermal history models of the Earth, and are inconsistent with an origin of the basalts from mantle plumes. The incompatible element and REE patterns of the basalts are distinct from the plume-derived mid-Proterozoic Mackenzie basalts of the Canadian Shield, the latter showing higher chondrite-normalized $Dy_N/Yb_N$ ratios indicative of melting of a garnet-bearing mantle source. By contrast, the lower $Dy_N/Yb_N$ ratios of all CDC/EDC and Cuddapah Basin basalts and flat REE patterns of their primary magmas indicate origin from a shallower, spinel-bearing mantle source. The basalts show LREE enrichment over HREE, and their $La_N/Sm_N$ ratios are higher than the $La_N/Sm_N$ ratios of the primary magmas, which can be attributed to upper crustal contamination. The estimated low potential temperatures, melting in the spinel lherzolite stability field, and the REE characteristics of the basalts and their primary magmas do not support an origin of the CDC/EDC and Cuddapah Basin basalts from mantle plumes.

**Supplementary Information** The online version contains supplementary material available at https://doi.org/10.1007/s00410-023-02012-0.

**Acknowledgements** This study is dedicated to late Prof. Somdev Bhattacharji who graciously provided the dike samples for this study. The samples were collected during a UNDP sponsored field trip. This manuscript greatly benefitted from detailed critical reviews by Wendy Bohrson, Richard Ernst and an anonymous reviewer. The constructive comments of the reviewers are greatly appreciated. Thoughtful comments and editorial handling by Othmar Müntener also helped to improve the presentation of the manuscript.

**Funding** Open Access funding provided by the MIT Libraries.

**Data availability** All data are available in the tables of the main text and in the electronic supplementary material.



## References

Aigner-Torres M, Blundy J, Ulmer P, Pettke T (2007) Laser Ablation ICPMS study of trace element partitioning between plagioclase and basaltic melts: an experimental approach. Contrib Mineral Petrol 153:647–667

Anand M, Gibson SA, Subbarao KV, Kelly SP, Dickin AP (2003) Early Proterozoic melt generation processes beneath the intracratonic Cuddapah Basin, southern India. J Petrol 44:2139–2171

Andersen DJ, Lindsley DH (1988) Internally consistent solution models for Fe-Mg-Mn-Ti spinels: Fe-Ti oxides. Amer Mineral 73:714–726

Annen C, Sparks RSJ (2002) Effects of repetitive emplacement of basaltic intrusions on thermal evolution and melt generation in the crust. Earth Planet Sci Lett 203:937–955

Armstrong JT (1995) CITZAF–a package for correction programs for the quantitative electron microbeam x-ray analysis of thick polished materials, thin-films and particles. Microbeam Anal 4:177–200

Babechuk MG, Widdowson M, Kamber BS (2014) Quantifying chemical weathering intensity and trace element release from two contrasting basalt profiles, Deccan Traps, India. Chem Geol 363:56–75

Baragar WRA, Ernst RE, Hulbert L, Peterson T (1996) Longitudinal petrochemical variation in the Mackenzie dyke swarm, northwestern Canadian Shield. J Petrol 37:317–359

Beattie P, Ford C, Russell D (1991) Partition coefficients for olivine-melt and orthopyroxene-melt systems. Contrib Mineral Petrol 109:212–224

Behn MD, Grove TL (2015) Melting systematics in mid-ocean ridge basalts: application of a plagioclase-spinel melting model to global variations in major element chemistry and crustal thickness. J Geophys Res Solid Earth 120:4863–4886. https://doi.org/10.1002/2015JB011885

Belica ME, Piispa EJ, Meert JG, Pesonen LJ, Plado J, Pandit MK, Kamenov GD, Celestino M (2014) Paleoproterozoic mafic dyke swarms from the Dharwar craton; paleomagnetic poles for India from 2.37 to 1.88 Ga and rethinking the Columbia supercontinent. Precamb Res 244:100–122

Bhattacharji S, Singh RN (1984) Thermomechanical structure of the southern part of the Indian shield and its relevance to Precambrian basin evolution. Tectonophys 105:103–120

Bhattacharji S (1987) Lineaments and igneous episodes in the evolution of intracratonic Proterozoic basins on the Indian Shield. In: Saha AK (ed.) Geological evolution of Peninsular India - petrological and structural aspects, Recent Researches in Geology. 13:1–15
Bindeman IN, Davis AM, Drake MJ (1998) Ion microprobe study of plagioclase-basalt partition experiments at natural concentration levels of trace elements. Geochim Cosmochim Acta 62(7):1175–1193
Blundy J, Melekhova E, Ziberna L, Humphreys MCS, Cerantola V, Brooker RA, McCammon CA, Pichavant M, Ulmer P (2020) Effect of redox on Fe–Mg–Mn exchange between olivine and melt and an oxybarometer for basalts. Contrib Mineral Pet 175:103
Bohrson WA, Spera FJ (2001) Energy-constrained open-system magmatic processes II: Application of energy-constrained assimilation-fractional crystallization (EC-AFC) model to magmatic systems. J Petrol 42:1019–1041
Chadwick B, Vasudev VN, Hegde GV (2000) The Dharwar craton, southern India, interpreted as the result of late Archean oblique convergence. Precamb Res 99:91–111
Chardon D, Jayananda M, Peucat J-J (2011) Lateral constrictional flow of hot orogenic crust: insights from the Neoarchean of south India, geological and geophysical implications for orogenic plateaux. Geochem Geophys Geosyst 12:Q02005
Chatterjee N (2021) Origin of the primitive, strongly $SiO_2$-undersaturated alkalic rocks from the Deccan Traps by low-degree mantle melting and high-pressure fractional crystallization. Contrib Mineral Petrol 176:31
Chatterjee N, Bhattacharji S (1998) Formation of Proterozoic tholeiite intrusives in and around Cuddapah Basin, south India and their Gondwana counterparts in east Antarctica: and compositional variation in their mantle sources. Neues Jb Miner Abh 174(1):79–102
Chatterjee N, Bhattacharji S (2001) Petrology, geochemistry and tectonic settings of the mafic dykes and sills associated with the evolution of the Proterozoic Cuddapah Basin of south India. Proc Indian Acad Sci (earth Planet Sci) 110:433–453
Chatterjee N, Sheth H (2015) Origin of the Powai ankaramite, and the composition, P-T conditions of equilibration and evolution of the primary magmas of the Deccan tholeiites. Contrib Mineral Petrol 169:32
Clark C, Collins AS, Timms NE, Kinny PD, Chetty TRK, Santosh M (2009) SHRIMP U-Pb age constraints on magmatism and high-grade metamorphism in the Salem Block, southern India. Gond Res 16(1):27–36
Collins AS, Patranabis-Deb S, Alexander E, Bertram CN, Falster GM, Gore RJ, Mackintosh J, Dhang PC, Saha D, Payne JL, Jourdan F, Backé G, Halverson GP, Wade BP (2015) Detrital mineral age, radiogenic isotopic stratigraphy and tectonic significance of the Cuddapah Basin, India. Gond Res 28:1294–1309
Condie KC (2005) High field strength element ratios in Archean basalts: a window to evolving sources of mantle plumes? Lithos 79:491–504
Das R, Saikia U, Rai SS (2015) The deep geology of South India inferred from Moho depth and Vp/Vs ratio. Geophys J Int 203:910–926. https://doi.org/10.1093/gji/ggv351
Davies GF (1999) Dynamic Earth: Plates. Cambridge University Press, Plumes and Mantle Convection, p 458
DePaolo DJ (1981) Trace element and isotopic effects of combined wall rock assimilation and fractional crystallization. Earth Planet Sci Lett 53:189–202
Ernst RE, Baragar WRA (1992) Evidence from magnetic fabric for the flow pattern of magma in the Mackenzie giant radiating dyke swarm. Nature 356:511–513
Ernst RE, Srivastava RK (2008) India's place in the Proterozoic world: constraints from the Large Igneous Province (LIP) record. In: Sivaji Ch, Chalapathi Rao NV (eds) Srivastava RK. Geochem, Geophys Geochron, Narosa Publ House Pvt Ltd, New Delhi, India pp, pp 41–56
Ernst RE, Liikane DA, Jowitt SM, Buchan KL, Blanchard JA (2019) A new plumbing system framework for mantle plume-related continental large igneous provinces and their mafic-ultramafic intrusions. J Volcanol Geotherm Res 384:75–84
French JE, Heaman LM (2010) Precise U-Pb dating of Paleoproterozoic mafic dyke swarms of the Dharwar craton, India: implications for the existence of the Neoarchean supercraton Sclavia. Precamb Res 183:416–441
French JE, Heaman LM, Chacko T, Srivastava RK (2008) 1891–1883 Ma Southern Bastar-Cuddapah mafic igneous events, India: a newly recognised large igneous province. Precamb Res 160:308–322
Friend CRL, Nutman AP (1991) SHRIMP U-Pb geochronology of the Closepet granite and peninsular gneiss, Karnataka, South India. J Geol Soc India 38:357–368
GERM (2022) Geochemical earth reference model partition coefficient (Kd) database. Earth Ref. org. https://kdd.earthref.org/KdD/
Ghosh JG, DeWit MJ, Zartman RE (2004) Age and tectonic evolution of Neoproterozoic ductile shear zones in the Southern Granulite Terrain of India, with implications for Gondwana studies. Tectonics 23(3):1–38. https://doi.org/10.1029/2002TC001444
Grove TL (1993) Corrections to expressions for calculating mineral components in "Origin of calc-alkaline series lavas at medicine lake volcano by fractionation, assimilation and mixing" and "Experimental petrology of normal MORB near the kane fracture zone: 22°–25°N, Mid-Atlantic Ridge." Contrib Mineral Petrol 114:422–424
Grove TL, Holbig ES, Barr JA, Till CB, Krawczynski MJ (2013) Melts of garnet lherzolite: experiments, models and comparison to melts of pyroxenite and carbonated lherzolite. Contrib Mineral Petrol 166:887–910. https://doi.org/10.1007/s00410-013-0899-9
Grove TL, Kinzler R, Bryan W (1992) Fractionation of mid-ocean ridge basalt (MORB). In: Phipps Morgan J, Blackman D, Sinton J (eds.) Mantle Flow and Melt Generation at Mid-Ocean Ridges. Geophys Monogr 71, AGU, Washington, DC, pp 281–310
GSI (1998) Geological Map of India. In: Dasgupta A, Chakravorty K (eds) Acharyya SK. Geol Surv India, Hyderabad
Gupta S, Rai SS, Prakasam KS, Srinagesh D, Bansal BK, Chadha RK, Priestley K, Gaur K (2003) The nature of the crust in southern India: implications for Precambrian crustal evolution. Geophys Res Lett. https://doi.org/10.1029/2002GL016770
Halls HC (1982) The importance and potential of mafic dyke swarms in studies of geodynamic processes. Geosci Canada 9:145–154
Halls HC, Kumar A, Srinivasan R, Hamilton MA (2007) Paleomagnetism and U-Pb geochronology of eastern trending dykes in the Dharwar craton, India: feldspar clouding, radiating dyke swarms and the position of India at 2.37 Ga. Precamb Res 155:47–68
Herzberg C (2022) Understanding the Paleoproterozoic Circum-Superior Large Igneous Province constrains the thermal properties of Earth's mantle through time. Precamb Res 375:106671
Herzberg C, Asimow PD, Arndt N, Niu Y, Lesher CM, Fitton JG, Cheadle MJ, Saunders AD (2007) Temperatures in ambient mantle and plumes: constraints from basalts, picrites and komatiites. Geochem Geophys Geosyst 8:Q02006. https://doi.org/10.1029/2006GC001390
Herzberg C, Condie K, Korenaga J (2010) Thermal history of the Earth and its petrological expression. Earth Planet Sci Lett 292:79–88
Higgins O, Sheldrake T, Caricchi L (2022) Machine learning thermobarometry and chemometry using amphibole and clinopyroxene: a window into the roots of an arc volcano (Mount Liamuiga,

Saint Kitts). Contrib Mineral Petrol 177:10. https://doi.org/10.1007/s00410-021-01874-6
Jayananda M, Banerjee M, Pant NC, Dasgupta S, Kano T, Mahesha N, Mahableswar B (2011) 262 Ga high-temperature metamorphism in the central part of the Eastern Dharwar Craton: implications for late Achaean tectonothermal history. Geol J. https://doi.org/10.1002/gj.1308
Jayananda M, Peucat JJ, Chardon D, Krishna Rao B, Corfu F (2013a) Neoarchean greenstone volcanism, Dharwar craton, Southern India: constraints from SIMS zircon geochronology and Nd isotopes. Precamb Res 227:55–76
Jayananda M, Tsutsumi Y, Miyazaki Y, Gireesh RV, Kapfo K-U, Tushipokla HH, Kano T (2013b) Geochronologic constraints on Meso and Neoarchean regional metamorphism and magmatism in the Dharwar craton, southern India. J Asian Earth Sci 78:18–38
Jayananda M, Santosh M, Aadhiseshan KR (2018) Formation of Archean (3600–2500 Ma) continental crust in the Dharwar Craton, southern India. Earth-Sci Rev 181:12–42
Johnson KTM, Kinzler RJ (1989) Partitioning of REE, Ti, Zr, Hf, and Nb between clinopyroxene and basaltic liquid: an ion microprobe study. Eos 70:1388
Jorgenson C, Higgins O, Petrelli M, Bégué F, Caricchi L (2022) A machine learning-based approach to clinopyroxene thermobarometry: Model optimization and distribution for use in Earth sciences. J Geophys Res. https://doi.org/10.1029/2021JB022904
Kinzler R, Grove TL (1992a) Primary magmas of mid-ocean ridge basalts, 1. Exp Res J Geophys Res 97:6885–6906. https://doi.org/10.1029/91JB02840
Kinzler RJ, Grove TL (1992b) Primary magmas of mid-ocean ridge basalts 2. Applications J Geophys Res 97:6907–6926
Kjøll HJ, Galland O, Labrousse L, Andersen TB (2019) Emplacement mechanisms of a dyke swarm across the brittle-ductile transition and the geodynamic implications for magma-rich margins. Earth Planet Sci Lett 518:223–235
Korenaga J (2008) Urey ratio and the structure and evolution of Earth's mantle. Rev Geophys. https://doi.org/10.1029/2007RG000241
Krein SB, Molitor ZJ, Grove TL (2021) ReversePetrogen: A Multiphase dry reverse fractional crystallization-mantle melting thermobarometer applied to 13589 mid-ocean ridge basalt glasses. J Geophys Res 126:e2020JB021292
Kumar A, Bhalla MS (1983) Palaeomagnetics and igneous activity of the area adjoining the southwestern margin of the Cuddapah basin. India Geophys J R Astron Soc 73:27–37
Kumar A, Hamilton MA, Halls HC (2012a) A Paleoproterozoic giant radiating dyke swarm in the Dharwar Craton, southern India. Geochem Geophys Geosyst 7:Q02011
Kumar A, Nagaraju E, Besse J, Bhaskar Rao YJ (2012b) New age, geochemical and paleomagnetic data on a 2.21 Ga dyke swarm from southern India: constraints on Paleoproterozoic reconstruction. Precamb Res 220–221:123–138
Kumar A, Parashuramulu V, Nagaraju E (2015) A 2082 Ma radiating dyke swarm in the Eastern Dharwar Craton, southern India and its implications to Cuddapah basin formation. Precamb Res 266:490–505
Le Bas MJ, Le Maitre RW, Streckeisen A, Zanettin B (1986) A chemical classification of volcanic rocks based on the total alkali-silica diagram. J Petrol 27:745–750
Liao AC-Y, Shellnutt JG, Hari KR, Denyszyn SW, Vishwakarma N, Verma CB (2019) A petrogenetic relationship between 2.37 Ga boninitic dyke swarms of the Indian Shield: evidence from the central Bastar Craton and the NE Dharwar Craton. Gond Res 69:193–211
Macdonald GA, Katsura T (1964) Chemical composition of Hawaiian lavas. J Petrol 5:82–133
Manikyamba C, Kerrich R (2012) Eastern Dharwar craton, India: continental lithosphere growth by accretion of diverse plume and arc terranes. Geosci Front 3:225–240
McDonough WF, Sun S-S (1995) Composition of the Earth. Chem Geol 120:223–253. https://doi.org/10.1016/0009-2541(94)00140-4
McKenzie D, Bickle MJ (1988) The volume and composition of melt generated by extension of the lithosphere. J Petrol 29:625–679
Mishra DC (2015) Plume and Plate Tectonics Model for formation of some Proterozoic Basins of India along Contemporary Mobile Belts: Mahakoshal – Bijawar, Vindhyan and Cuddapah Basins. J Geol Soc India 85:525–536
Mohanty S (2011) Palaeoproterozoic assembly of the Napier Complex, Southern India and Western Australia: Implications for the evolution of the Cuddapah basin. Gond Res 20:344–361. https://doi.org/10.1016/j.gr.2011.03.009
Moore NE, Grunder AL, Bohrson WA (2018) The three-stage petrochemical evolution of the Steens Basalt compared to large igneous provinces and layered mafic intrusions. Geosphere 14(6):2505–2532. https://doi.org/10.1130/GES01665.1
Moore NE, Grunder AL, Bohrson WA, Carlson RW, Bindeman IN (2020) Changing mantle sources and the effects of crustal passage on the Steens Basalt SE Oregon chemical and isotopic constraints. Geochem Geophys Geosyst. https://doi.org/10.1029/2020GC008910
Morgan WJ (1971) Convection plumes in the lower mantle. Nature 230:42–43
Murty YGK, Babu Rao V, Guptasarma D, Rao JM, Rao MN, Bhattacharji S (1987) Tectonic, petrochemical and geophysical studies of mafic dyke swarms around the Proterozoic Cuddapah Basin, south India. In: Halls HC, Fahrig W (eds.) Mafic Dyke Swarms. Geol Assoc Canada Spl Paper 34:303–316
Nagaraja Rao BK, Rajurkar ST, Ramlingaswamy G, Ravindra Babu B (1987) Stratigraphy, structure and evolution of the Cuddapah basin. In: Radhakrishna BP (ed.) Purana Basins of Peninsular India (Middle to Late Proterozoic). Mem Geol Soc India 6:33–86
Nagaraju E, Parashuramulu V, Ramesh Babu N, Narayana AC (2018a) A 2207 Ma radiating mafic dyke swarm from eastern Dharwar craton, Southern India: drift history through Paleoproterozoic. Precamb Res 317:89–100
Nagaraju E, Parashuramulu V, Kumar A, Srinivas Sarma D (2018b) Paleomagnetism and geochronological studies on a 450 km long 2216 Ma dyke from the Dharwar craton, southern India. Phys Earth Planet Inter 274:222–231
Naqvi SM, Rogers JJW (1987) Precambrian Geology of India. Oxford Univ Press Inc 223 p.
Nesbitt HW, Young GM (1982) Early Proterozoic climates and plate motions inferred from major element chemistry of lutites. Nature 299:715–717
NGRI (1978) Gravity map series of India. National Geophysical Research Institute, Hyderabad, India, NGRI-GPH/2, 1 sheet 1:5000000
Padmakumari VM, Dayal AM (1987) Geochronological studies of some mafic dykes around the Cuddapah basin, south India. In: Radhakrishna BP (Ed.) Purana Basins of Peninsular India (Middle to Late Proterozoic). Geol Soc India Memoir 6, pp. 369–373
Pearce JA (2008) Geochemical fingerprinting of oceanic basalts with applications to ophiolite classification and the search for Archean oceanic crust. Lithos 100:14–48
Peucat J-J, Jayananda M, Chardon D, Capdevila R, Fanning Marc C, Paquette J-L (2013) The lower crust of Dharwar craton, south India: patchwork of Archean granulitic domains. Precamb Res 227:4–29
Poornachandra Rao GVS (2005) Orthogonal dykes around the Cuddapah basin - a paleomagnetic study. J Indian Geophys Union 9:1–11

Presnall DC, Gudfinnsson GH, Walter MJ (2002) Generation of mid-ocean ridge basalts at pressures from 1 to 7 GPa. Geochim Cosmochim Acta 66:2073–2090

Putirka KD (2008) Thermometers and barometers for volcanic systems. Rev Mineral Geochem 69:61–120

Putirka KD (2016a) Rates and styles of planetary cooling on earth, moon, mars, and vesta, using new models for oxygen fugacity, ferric-ferrous ratios, olivine-liquid Fe-Mg exchange, and mantle potential temperature. Amer Mineral 101:819–840

Putirka KD (2016b) Amphibole thermometers and barometers for igneous systems and some implications for eruption mechanisms of felsic magmas at arc volcanoes. Amer Mineral 101:841–858

Putirka K, Johnson M, Kinzler R, Walker D (1996) Thermobarometry of mafic igneous rocks based on clinopyroxene-liquid equilibria, 0–30 kbar. Contrib Mineral Petrol 123:92–108

Putirka KD, Perfit M, Ryerson FJ, Jackson MG (2007) Ambient and excess mantle temperatures, olivine thermometry, and active vs. passive upwelling. Chem Geol 241:177–206

Radhakrishna T, Joseph M (1996) Proterozoic paleomagnetism of the mafic dyke swarms in the high grade region of southern India. Precamb Res 76:31–46

Rajamani V, Shivkumar K, Hanson GN, Shirey SB (1985) Geochemistry and petrogenesis of amphibolites, Kolar Schist Belt, South India: Evidence for komatiitic magma derived by low percentages of melting of the mantle. J Petrol 26(1):92–123

Rao JM, Bhattacharji S, Rao MN, Hermes OD (1995) $^{40}Ar$-$^{39}Ar$ ages and geochemical characteristics of dolerite dykes around the Proterozoic Cuddapah basin, south India. Mem Geol Soc India 33:307–328

Rivalta E, Taisne B, Bunger AP, Katz RF (2015) A review of mechanical models of dike propagation: schools of thought, results and future directions. Tectonophys 638:1–42

Roeder PL, Emslie RF (1970) Olivine liquid equilibrium. Contrib Mineral Petrol 29:275–289

Rogers AJ, Kolb J, Meyer FM, Armstrong RA (2007) Tectono-magmatic evolution of the Hutti-Maski greenstone belt, India: constrained using geochemical and geochronological data. J Asian Earth Sci 31:55–70

Samal AK, Srivastava RK, Ernst RE (2021) An appraisal of mineral systems associated with Precambrian large igneous provinces of the Indian shield. Ore Geol Rev 131:104009

Shellnutt JG, Hari KR, Liao AC-Y, Denyszyn SW, Vishwakarma N (2018) A 1.88 Ga giant radiating mafic dyke swarm across southern India and Western Australia. Precamb Res 308:58–74

Sheppard S, Rasmussen B, Zi J-W, Somasekhar V, Sarma DS, Ram Mohan M, Krapež B, Wilde SA, McNaughton NJ (2017) Sedimentation and magmatism in the Paleoproterozoic Cuddapah Basin, India: consequences of lithospheric extension. Gond Res 48:153–163

Singh AP, Mishra DC, Gupta SB, Rao MRKP (2004) Crustal structure and domain tectonics of the Dharwar Craton (India): insight from new gravity data. J Asian Earth Sci 23:141–152

Sleep NH (1990) Hotspots and mantle plumes: some phenomenology. J Geophys Res 95:6715–6736

Söderlund U, Bleeker W, Demirer K, Srivastava RK, Hamilton M, Nilsson M, Pesonen LJ, Samal AK, Jayananda M, Ernst RE, Srinivas M (2019) Dharwar craton, India: Implications for paleoreconstructions and support for a ~30° change in dyke trends from south to north. Precamb Res 329:26–43

Spera FJ, Bohrson WA (2001) Energy-constrained open-system magmatic processes I: general model and energy-constrained assimilation and fractional crystallization (EC-AFC) formulation. J Petrol 42:999–1018. https://doi.org/10.1093/petrology/42.5.999

Srivastava RK, Jayananda M, Gautam GC, Gireesh V, Samal AK (2014a) Geochemistry of an ENE–WSW to NE–SW trending ~2.37 Ga mafic dyke swarm of the Eastern Dharwar Craton India: does it represent a single magmatic event? Chem Erde Geochem. 74:251–265

Srivastava RK, Jayananda M, Gautam GC, Samal AK (2014b) ~2.21–2.22 Ga N-S to NNW–SSE trending Kunigal mafic dyke swarm from Eastern Dharwar Craton, India: implications for Paleoproterozoic large igneous provinces and supercraton Superia. Mineral Petrol 109:695–711

Srivastava RK, Samal AK, Gautam GC (2015) Geochemical characteristics and petrogenesis of four Palaeoproterozoic mafic dyke swarms and associated large igneous provinces from the eastern Dharwar craton, India. Intern Geol Rev 57:1462–1484

Stark JC, Wang X-C, Denyszyn SW, Li Z-X, Rasmussen B, Zi J-W, Sheppard S, Liu Y (2019) Newly identified 1.89 Ga mafic dyke swarm in the Archean Yilgarn Craton, Western Australia suggests a connection with India. Precamb Res 329:156–169

Swami Nath J, Ramakrishnan M, Viswanatha MN (1976) Dharwar stratigraphic model and Karnataka craton evolution. Geol Surv India Records 107:149–175

Taylor SR, McLennan SM (1995) The geochemical evolution of the continental crust. Rev Geophys 33:241–265

Thompson AB, Matile L, Ulmer P (2002) Some thermal constraints on crustal assimilation during fractionation of hydrous, mantle-derived magmas with examples from central Alpine batholiths. J Petrol 43:403–422

Till CB (2017) A review and update of mantle thermobarometry for primitive arc magmas. Amer Mineral 102:931–947

Till CB, Grove TL, Krawczynski MJ (2012) A melting model for variably metasomatized plagioclase and spinel lherzolite. J Geophys Res 117:B06206. https://doi.org/10.1029/2011JB009044

Till CB, Grove TL, Carlson RW, Fouch MJ, Donnelly-Nolan JM, Wagner LS, Hart WK (2013) Depths and temperatures of <10.5 Ma mantle melting and the lithosphere-asthenosphere boundary below southern Oregon and northern California. Geochem Geophys Geosyst 14:864–879. https://doi.org/10.1002/ggge.20070

Tormey DR, Grove TL, Bryan WB (1987) Experimental petrology of normal MORB near the Kane fracture zone: 22–25°N, mid-Atlantic Ridge. Contrib Mineral Petrol 96:121–139

Watson S, McKenzie D (1991) Melt generation by plumes; a study of Hawaiian volcanism. J Petrol 32:501–537

White WM (2010) Oceanic island basalts and mantle plumes: the geochemical perspective. Annu Rev Earth Planet Sci 38:133–160

Yang HJ, Kinzler RJ, Grove TL (1996) Experiments and models of anhydrous, basaltic olivine-plagioclase-augite saturated melts from 0.001 to 10 kbar. Contrib Mineral Petrol 124:1–18